Elsevier Editorial System(tm) for Applied Catalysis B: Environmental

Manuscript Draft

Manuscript Number: APCATB-D-15-01427R1

Title: Engineering of oxoclusters-reinforced polymeric materials with application as heterogeneous oxydesulfurization catalysts

Article Type: Research Paper

Keywords: oxoclusters; hybrid materials; hydrogen peroxide; oxydesulfurization; solid state NMR

Corresponding Author: Dr. Mauro CARRARO,

Corresponding Author's Institution: Universita di Padova

First Author: Marilisa Vigolo

Order of Authors: Marilisa Vigolo; Silvia Borsacchi; Antonio Sorarù; Marco Geppi; Bernd Smarsly; Paolo Dolcet; Silvia Rizzato; Mauro CARRARO; Silvia Gross

Applied Catalysis B: Environmental
journal homepage: www.elsevier.com

Engineering of oxoclusters - reinforced polymeric materials with application as heterogeneous oxydesulfurization catalysts

Marilisa Vigolo[a,b], Silvia Borsacchi[b,c], Antonio Sorarù[a], Marco Geppi[b,c,d], Bernd Smarsly[e], Paolo Dolcet[a,b,f], Silvia Rizzato[g], Mauro Carraro* [a, h], Silvia Gross*[a,b,f]

[a] *Dipartimento di Scienze Chimiche, Università degli Studi di Padova, via Marzolo, 1, I-35131, Padova, Italy*
[b] *INSTM, Consorzio Interuniversitario per la Scienza e Tecnologia dei Materiali, via Giusti 9, 50121, Firenze, Italy*
[c] *Istituto di Chimica dei Composti Organometallici del Consiglio Nazionale delle Ricerche, Area della Ricerca di Pisa-S. Cataldo, Via G. Moruzzi 1, 56124 Pisa, Italy*
[d] *Dipartimento di Chimica e Chimica Industriale, Università di Pisa, via G. Moruzzi 13, 56124 Pisa, Italy*
[e] *P hysikalisch-Chemisches Institut, Justus-Liebig-Universität Giessen, Heinrich-Buff-Ring 58, D-35392 Giessen, Germany*
[f] *Istituto per l'Energetica e le Interfasi, IENI-CNR via Marzolo, 1, I-35131, Padova, Italy*
[g] *Dipartimento di Chimica, Università degli Studi di Milano, via Golgi, 9, I-20133, Milano, Italy*
[h] *Istituto per la Tecnologia delle Membrane, ITM-CNR via Marzolo, 1, I-35131, Padova, Italy*
* *E-mail; mauro.carraro@unipd.it; silvia.gross@unipd.it*

Dedicated to the memory of our friend and colleague Prof. Alessandro Bagno, Full Professor of Organic Chemistry at the University of Padova, unexpectedly and prematurely passed away on 23.3.2015

ARTICLE INFO

Article history:
Received
Received in revised form
Accepted
Available online

Keywords:
oxoclusters
hybrid materials
peroxides
DBT oxidation
Solid State NMR

ABSTRACT

In this paper we report the first example of hybrid materials based on polymethlymethacrylate (PMMA) matrices covalently reinforced by $M_yO_x(OH)_w(O(O)CR)_z$ oxoclusters (M=Zr or Hf), used as heterogeneous catalytic systems for hydrogen peroxide activation. The resulting hybrids were used to catalyze the oxidation of dibenzothiophene (DBT) to the corresponding sulfoxide (DBTO) and sulfone ($DBTO_2$), in order to demonstrate their potential application for the oxydesulfurization (ODS) of a fuel. Thanks to catalyst confinement and to the higher affinity of the polymeric matrix towards polar substrates, the heterogeneous set-up displays improved performances with respect to the corresponding homogeneous systems. At 65°C, a DBT conversion higher than 84% was obtained in 24 h, with a >94% selectivity for $DBTO_2$. The stability of the hybrid materials under catalytic conditions was successfully assessed by a combined spectroscopic approach, based on FT-IR, resonance Raman, Solid State Nuclear Magnetic Resonance, X-ray Absorption and Small Angle X-ray scattering measurements.

1. Introduction

Oxoclusters of early transition metals are a versatile class of polynuclear compounds built up of a limited number of 3-5 groups metal atoms, such as Ti^{IV}, Zr^{IV}, Hf^{IV} or Nb^{V}, linked by oxygen bridges and coordinated by organic ligands [1,2]. These compounds are globally neutral and discrete species with general formula $M_yO_x(OH)_w(O(O)CR)_z$, where typically organic carboxylates act as bidentate ligands. They can display different nuclearities (i.e. number of constituent metal atoms, y = 2–12), coordination number of the metal atoms (varying between 6 and 9) and connectivity modes (corner, edge or face sharing of polyhedral units). In some cases they also involve an alkaline earth (e.g. Ba, Mg) metal [3].

Since these oxoclusters are characterized by the presence of early transition metals in their highest oxidation state, they are appealing candidates as catalysts for peroxide activation [4,5]. Moreover, Zr and Hf-based multimetallic complexes have been reported to activate hydrogen peroxide, promoting the oxidation of different substrates (sulfides and sulfoxides, alcohols) both in water and in organic solvents [6–11]. As far as zirconium-based oxoclusters are concerned, we have recently evidenced the possibility to use two different complexes to activate hydrogen peroxide and oxidize organic substrates [12]. In such preliminary study, the oxidation of methyl *p*-tolylsulfide to the corresponding sulfoxide and sulfone was chosen as model reaction, showing an interesting reactivity towards sulfoxide oxidation [13]. However, despite the encouraging results, the hydrolytic stability of such oxoclusters is too low to allow a practical application in homogeneous catalysis, since they easily rearrange and precipitate from the reaction mixture.

Owing to the possibility to use oxoclusters as building blocks for the synthesis of different typologies of hybrid materials [14] with enhanced functional (e.g. dielectric, magnetic etc.) and

structural (thermal, mechanical) properties [15], we have devised novel heterogeneous systems based on the covalent immobilization of Zr and Hf oxoclusters into a polymeric matrix.

The protection of a catalytically active system by embedding/anchoring it within a matrix is an underlying and widely used strategy in heterogeneous catalysis [16]. Within this scenario, the preparation of hybrid materials through the integration of the multimetallic catalytic active species into a polymeric matrix is a fertile field of research [17–20]. Indeed, this strategy offers interesting perspectives for devising continuous flow processes, where the polymer may contribute to improve the reaction selectivity and/or enable process intensification, by coupling catalysis and separation technologies [20,21]. Nevertheless, to the best of our knowledge, the hybrid materials here described are the first example of heterogeneous catalysts based on the covalent immobilization of oxoclusters. Not only the covalent bonds endow the final material with enhanced stability, but also prevent phases separation inside the polymer matrix and leaching.

In this framework, different acrylate copolymers were prepared by changing the nature of the oxocluster as well as the oxocluster/monomer molar ratio, which in turn, *inter alia*, affect the cross-linking degree of the resulting hybrid. The effectiveness of the hybrid materials as heterogeneous catalysts was evaluated in the oxidation of an aromatic sulfide by H_2O_2, in a biphasic *n*-octane/acetonitrile system, as an example of sustainable fuel desulfurization process [22,23]. In particular, we exploited the oxocluster reactivity to perform the oxidation of dibenzothiophene (DBT), dissolved in *n*-octane, to the corresponding sulfoxide (DBTO) and sulfone ($DBTO_2$), whereby the oxidized products can be easily extracted by the polar solvent [20]. Thanks to the enhanced affinity of the polymeric matrix toward polar substrates and solvents, the heterogeneous set-up shows better performances than the corresponding homogeneous systems. Furthermore, the heterogeneous catalysts can be recovered and reused. FT-IR, resonance Raman, Solid State Nuclear Magnetic Resonance (SS-NMR), X-ray Absorption (XAS), and Small Angle X-ray scattering measurements (SAXS) highlighted, indeed, that the hybrids are endowed with appreciable stability even after catalytic turnover.

2. Experimental

2.1. Materials and chemicals

Zirconium butoxide ($Zr(O^nBu)_4$, 80% wt in *n*-butanol), zirconium propoxide ($Zr(O^nPr)_4$) 70% wt in *n*-propanol), vinylacetic acid, dibenzothiophene (DBT), dibenzothiophene sulfone ($DBTO_2$), hydrogen peroxide (30% wt in water) were all purchased from Sigma-Aldrich and used as received. Hafnium butoxide ($Hf(O^nBu)_4$, 95% wt in *n*-butanol) was supplied by ABCR. Methacrylic acid 99%, and methymethacrylate, purchased from Sigma-Aldrich, were filtered on neutral alumina to remove the inhibitor. All the chemicals were stored under argon, while the solvents were additionally stored on molecular sieves. Dibenzothiophene sulfoxide (DBTO) was synthesized following a literature procedure [24]. Oxoclusters $M_4O_2(O(O)CC(CH_3)=CH_2)_{12}$ (Hf_4, with M=Hf) [25] or (Zr_4, with M=Zr) [26], $Zr_6(OH)_4O_4(O(O)CC(CH_3)=CH_2)_{12}$ (Zr_6) [27], $[Zr_6O_4(OH)_4(O(O)CCH_2CH=CH_2)_{12}]_2\cdot 6CH_2=CHCH_2C(O)OH$ (Zr_{12}) [28], were synthesized under argon, using standard Schlenk techniques, according to literature procedures. The structure of all oxoclusters was confirmed by measuring the unit cell dimensions on a number of different single crystals by diffraction technique. Moreover, the nature of the bulk precipitate formed by a mixture of single crystals and an apparently amorphous solid has been investigated by X-ray powder diffraction techniques, by comparison with the spectra simulated from the single crystal data that has confirmed the purity of the products.

2.2. Hybrid materials syntheses

The hybrid materials were prepared by implementing a known procedure [29]. In a typical polymerization, a weighed amount (0.7 g, moles amount depending on the oxocluster) of oxocluster was dissolved in methyl methacrylate (3-12 g), so to achieve oxocluster : MMA molar ratios of 1:50, 1:100, and 1:200. The thermoinitiator benzoylperoxide (BPO) (3% wt. with respect to the monomer) was finally added to the suspension and the reaction mixture was heated at 80°C for 1 h. Glassy monolithic materials were thus obtained. Samples were labeled as M_xMMAnT with M=Zr and x=4, 6 or 12, or M=Hf and x=4, n (molar ratio) = 50, 100 or 200, while T stands for thermal polymerization. Reference PMMA (poly methyl methacrylate) was prepared by using the same procedure, without adding the oxocluster. Porogenic solvents (1,4-butandiol and 2-propanol, 1:2 v/v) were added to the reaction mixture to produce porous polymers. In this latter case, samples were labeled as M_xMMAnP.

2.3. Solid State NMR measurements

^{13}C SS-NMR spectra were recorded on a Varian InfinityPlus 400 spectrometer, working at a Larmor frequency of 400.02 MHz and 100.59 MHz for proton and carbon nuclei, respectively, using a 7.5 mm probehead with a 90° 1H pulse duration of 5 μs. ^{13}C Cross Polarization-Magic Angle Spinning (CP-MAS) spectra were recorded with high-power decoupling from ^1H nuclei, spinning the samples at a MAS frequency between 5 and 6 kHz (depending on the sample), using a contact time of 1 ms, a recycle delay of 5 s and accumulating 10000 transients. The ^{13}C chemical shift scale was calibrated using hexamethylbenzene and TMS as secondary and primary references, respectively. All the spectra were recorded at 25 °C, using air as spinning gas.

2.4. XAS measurements

Synchrotron (Trieste, Italy). A Si(311) double crystal monochromator was used for measurements at the Zr K-edge (17.998 keV). The second monochromator crystal was tilted for optimal harmonic rejection. The spectra were recorded in transmission mode using ionization chambers as detectors. Energy calibration was performed with a Zr metal foil. The solid samples were pressed into self-supporting pellets using cellulose as a binder.

Data evaluation started with background absorption removal from the experimental absorption spectrum by using the automated removal routine found in the Athena software [30]. The threshold energy E_0 was determined as the maximum in the first derivative spectrum. To determine the smooth part of the spectrum, corrected for pre-edge absorption, a piecewise polynomial was used. It was adjusted in such a way that the low-R components of the resulting Fourier transform were minimal. After division of the background–subtracted spectrum by its smooth part, the photon energy was converted to photoelectron wave numbers k. The resulting $\chi(k)$-function was weighted with k^3 and Fourier transformed using a Hanning window function.

Data analysis was performed in k-space on unfiltered data, using the Artemis software [30].

2.5. SAXS measurements

SAXS patterns were recorded employing a Nonius rotating anode generator equipped with a 3 pin-hole setup (installed at Max-Planck-Institute of Colloids and interfaces) providing a wavelength of $\lambda = 0.154$ nm (CuK_α radiation), and using a MAR CCD area-detector. The 2D SAXS patterns were radially averaged, providing 1D SAXS intensity scans as a function of the modulus of the scattering vector $s = 2/\lambda \sin(\theta)$, where 2θ is the scattering angle.

2.6. SEM measurements

Scanning Electron Microscopy measurements were performed using a field emission SEM, Zeiss SUPRA 40VP equipped with an EDXS system (Oxford INCA), by using a primary beam acceleration voltage of 10 kV.

2.7. FT-IR measurements

Infrared spectra were collected by using a Thermo Quest Nicolet 5700 instrument. Few milligram of oxocluster before and after catalysis were dispersed into KBr pellets.

2.8. Inductively coupled plasma - mass spectrometry (ICP-MS)

An ICP-MS Agilent Technologies 7700 instrument, operating at 1550 W plasma power was used to detect the amount of Zr released in solution. A CEM Discover SP-D microwave reactor was used for the microwave assisted acid (HNO_3+HF 7:1) digestion of the samples. The instrumental operating conditions were as follows: T_{max} = 180 °C, ramp time = 4 min, stop time = 10 min, power = 300 W.

2.9. Raman measurements

Raman spectra were collected by using a Thermo DXR Raman Microscope. A 780 nm laser was used as excitation source, operated at a power of 24 mW.

2.10. Catalytic tests

For the oxidation reactions, the oxocluster (1.5 μmol) was dissolved in CH_3CN (1 ml) and mixed with a *n*-octane solution (1 ml) containing DBT (10 μmol). The biphasic systems were stirred for 5 min before adding H_2O_2 (35 μmol, added as 30% aq. solution). The reactions were performed at 65°C and monitored over 24 h. H_2O_2 consumption was verified by iodinated paper. Samples (20 μL) of both phases were withdrawn at fixed time interval, diluted in a CH_3CN solution, containing 9-fluorenone as chromatographic standard, and treated with supported triphenylphosphine as oxidant quencher. The samples were then filtered on membrane filters (0.45 μm) and analyzed by HPLC, using a Gemini C18 column (Phenomenex) eluted (1 mL min^{-1}) with the following solvent gradient: H_2O/CH_3CN (40:60) for 2 min, 100% CH_3CN at 9 min; the UV detector was set at λ= 220 nm.

In all reactions, the amount of material was established in order to provide the same amount of oxoclusters. The hybrid polymers were used as grinded powder.

Catalyst stability and its recycling were assessed by (i) recharging the reaction mixture with further aliquots of DBT and H_2O_2, (ii) reusing the recovered catalyst, after centrifugation and washing with acetonitrile, (iii) by checking the residual reactivity of the reaction mixture after removal by filtration of the oxocluster. The recovered catalysts, labeled as M_xMMAnA were analyzed by FTIR, Raman, ^{13}C CP-MAS spectra.
Blank reactions were performed without catalyst as well as by using the methacrylic acid, to exclude the formation of peracids.

2.11. Swellings

The swelling experiments were carried out by simply leaving carefully weighted normalized samples of polymers in ethylacetate and water for 72 hours. Then the percentage weight increase of all the samples was determined and the swelling index (I_{sw}) could be calculated according to [31–33]:

I_{sw} = wet weight- dry weight/dry weight

3. Results and discussion

3.1. Synthesis and characterization of the oxocluster-based organic inorganic hybrid materials.

The hybrid materials were synthesized by implementing a previously published procedure, based on the copolymerization of the methacrylate- or vinylacetate [34] functionalized oxoclusters with methlymethacrylate (MMA) monomers, to give an oxocluster-reinforced polymeric matrix.

In particular, the nature of the oxocluster as well as its molar ratio with respect to the monomers were systematically varied in the preparation of the hybrids, in order to assess their effect on the catalytic properties. In the following Table 1, the prepared samples and their composition are collected.

Table 1. Samples labelling and swelling data.

Sample name	Oxocluster/monomer molar ratio	Swelling[a]
Zr_4MMA50T	1:50	59
Zr_4MMA100T	1:100	100
Zr_4MMA200T	1:200	209
Zr_6MMA50T	1:50	39
Zr_6MMA100T	1:100	54
Zr_6MMA200T	1:200	100
Zr_{12}MMA50T	1:50	56
Zr_{12}MMA100T	1:100	- [b]
Zr_{12}MMA200T	1:200	- [b]
Hf_4MMA50T	1:50	50

[a] Calculated after 72 h in ethylacetate. [b] The material is soluble.

The materials were firstly characterized to confirm the presence of the oxoclusters and to investigate the possible presence of residual double bonds, in order to assess the

polymerization degree. Due to the overwhelming contribution of the PMMA matrix, all FT-IR spectra appear very similar each other (See Fig.1), with C=O stretching of the ester group at about 1720 cm^{-1} and aliphatic C-H stretchings at about 2900 cm^{-1}. In the region 1400-1590 cm^{-1}, vibrations ascribable to the symmetric and asymmetric stretchings of the carboxylate groups coordinated to the oxocluster metal ions can be detected [35]. The presence of low intensity vibrational bands at 1640 cm^{-1} hints to the presence of a small quantity of unreacted C=C double bonds, belonging to the oxocluster as well as to the monomer. The presence of these residual double bonds can be ascribed to the high steric hindrance of the oxoclusters, bearing 12 or 24 polymerizable groups which, once the copolymerization has been started, remain embedded in a stiff structure, thus preventing their reaction with further monomers.

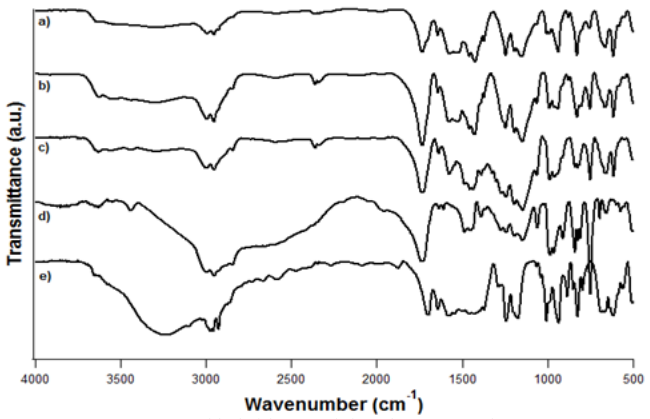

Fig. 1. FT-IR spectra of hybrids containing the Zr_6 oxocluster: [Zr_6MMA50T (a), Zr_6MMA100T (b) and Zr_6MMA200T (c)], compared to PMMA (d) and pure Zr_6 oxocluster (e). To allow an easier recognition of Zr_6-based oxocluster signals, the spectrum of the PMMA matrix was subtracted from their spectra (see Fig. S1).

The thermal behavior of the materials was then investigated by thermogravimetry. The recorded data confirm previous findings [26] about the improved thermal stability of the polymers cross-linked by the oxoclusters with respect to pristine PMMA, being the stability directly related to the oxocluster content (Fig. S2-S4). In the case of Zr-based oxoclusters (Fig.S2), thermogravimetric curves pointed out that a first weight loss (ca. 13%) occurs in the range 200-300°C, assigned to the removal of residual monomer and other adsorbed species, whereas at higher temperatures (300-450°C) a more relevant weight loss is observed, which has to be ascribed to the degradation of the hybrid matrix. At temperatures higher than 400°C, a last weight loss is detected, due to the decomposition of the organic part of the oxocluster to give ZrO_2, which is the detected inorganic residue observed (about 10-12% of the initial weight, in agreement to the amount of embedded oxocluster, each mole of which by decomposing produces 4 moles of zirconia).

The higher thermal stability of the hybrid materials is highlighted by the different degradation profiles (Fig. S2), being anticipated by about 80°C for the oxocluster-free PMMA. This effect is due to the enhanced cross-linking degree, induced by the oxocluster, as well as to the refractory layer produced, during combustion, by the inorganic domains as filler [36]. Accordingly, the highest thermal stability is displayed by Zr_4MMA50T, which is the sample characterized by the highest amount of incorporated oxocluster.

Upon storage in ethylacetate for 72 hours, the cross-linked materials swell (Table 1), the degree of swelling being related to the amount of incorporated oxocluster (i.e. the higher the amount of oxocluster, the higher the cross-linking, the lower the swelling degree). On the other hand, pristine PMMA and the hybrid materials embedding Zr_{12} completely dissolved. This latter observation can be related, as evidenced by the SS-NMR data (*vide infra*), to the fact that these bigger twelve-metals oxoclusters cross-link much less efficiently the polymer matrix, and they are loosely linked to it.

With the aim of obtaining further and more detailed structural information on the prepared hybrids, ^{13}C CP-MAS NMR spectra were recorded on Zr_4MMA50T, Zr_6MMA50T, Zr_{12}MMA50T, on the respective starting oxoclusters (Zr_4, Zr_6, Zr_{12}) and on PMMA. In Fig. 2 the spectra of all these samples are shown. The comparison with the spectra of pristine Zr_4 and PMMA provides information on the modifications occurring upon the hybrid formation. PMMA signals in the spectra of the hybrid and of pristine polymer appear substantially identical, indicating the similarity of the main structural features of PMMA in the presence or absence of the oxoclusters. In the spectrum of the pristine oxocluster Zr_4, every signal corresponding to a certain carbon nucleus appears structured in a variable number of peaks. Indeed, as shown by the crystal structure of Zr_4, [26,37] methacrylate groups occupy several spatially non-equivalent positions.

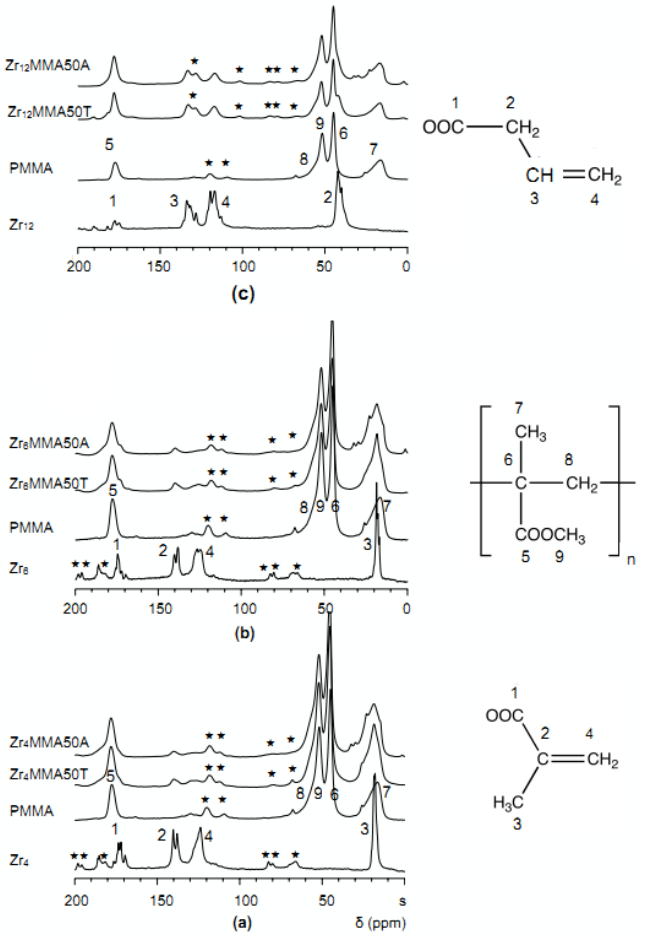

Fig. 2. ^{13}C CP-MAS spectra of (a) Zr_4, PMMA, hybrid Zr_4MMA50T before and after (Zr_4MMA50A) the reaction; (b) Zr_6, PMMA, hybrid Zr_6MMA50T before and after (Zr_6MMA50A) the reaction; (c) Zr_{12}, PMMA, hybrid Zr_{12}MMA50T before and after (Zr_{12}MMA50A) the reaction. The structures of the methacrylate group and methylmethacrylate, as monomers and as polymers are also reported, with the carbons numbering used for the signals assignment. Stars indicate spinning sidebands.

On the other hand, the broader signals observed for the embedded oxocluster suggest a higher degree of disorder for methacrylate

groups dispersed in the polymer matrix. In detail, the broad signal at about 18 ppm arises from the superposition of the intrinsically broad methyl signal of PMMA and of the narrow one belonging to methyl groups on Zr_4. The main chain ^{13}C signals of PMMA appear between 40 and 60 ppm, together with that of the methoxy carbon atoms [38–40].

Between 120 and 140 ppm, thanks to a spectral fitting procedure (the results of which are reported in Fig. S5), three signals can be recognized. Two of them, at 125 and 140 ppm, are ascribable to the olefinic carbons of Zr_4, and the last one, at about 130 ppm is due to olefinic carbon atoms of MMA (unreacted double bonds), and it is also observed in the spectrum of PMMA.

The COO ester group signal of PMMA is observed at 178 ppm, while two weak and broad shoulders, for the hybrids, are ascribable to the carboxylic carbon atoms of Zr_4. To estimate the amount of unreacted olefinic carbon atoms, and assess the polymerization degree, a quantitative ^{13}C DE-MAS spectrum of the hybrid was recorded (Fig.S5), from which it results that about 10-20% of MMA double bonds and about 50% of Zr_4 double bonds does not react, in agreement with FT-IR findings. This can also account for the TGA observation that 10-20% of the initial monomer is not incorporated, nevertheless hinting at a good degree of copolymerization.

The spectrum of Zr_6MMA50T is similar to that of Zr_4MMA50T, and all the comments done so far substantially hold true. A quantitative DE-MAS spectrum, due to the extremely long time required, was not recorded but, by applying approximate scaling factors (obtained from the spectra of Zr_4MMA50T) to the signals area of the CP-MAS spectrum, it was possible to estimate that also in this case about 50% of the oxocluster double bonds did not take part to the hybrid formation.

The case of Zr_{12}MMA50T is different since the oxocluster is functionalized with vinylacetate rather than methacrylate groups, and the potentially polymerizable groups are 24 instead of 12. Indeed, in the spectrum of the oxocluster, a signal at about 40 ppm, due to $OOCCH_2$- carbon is present and the peaks of the other carbon nuclei, which are characterized by a noticeable multiplicity, appear at slightly different chemical shifts with respect to Zr_4 and Zr_6. Concerning olefinic carbons of unreacted double bonds of both MMA and Zr_{12} it appears, from an approximate quantitative estimate (performed as previously discussed for Zr_6MMA50T), that more than 90% of the oxocluster double bonds does not react in the hybrid formation, output that also in this case can be traced back to steric hindrance, and which correlates well with the qualitative swelling experiments, showing that the hybrid materials embedding this oxocluster completely dissolve, hinting at a scarcely cross-linked structure.

3.2. Catalytic tests

Once thoroughly characterized from the chemico-physical and structural point of view, the obtained materials were tested in a model catalytic reaction, by exploiting the presence of Zr^{IV} and Hf^{IV} centers to activate hydrogen peroxide. A previous study on zirconium-based oxoclusters with interesting activity towards the oxygenation of sulfides and sulfoxides [12] has encouraged us to explore the double phase oxydesulfurization (ODS) of a model fuel in the presence of the polymeric materials embedding the oxoclusters. The oxidative removal of sulfur compounds may represent a sustainable alternative to the traditional hydrodesulfurization (HDS) process, since it can operate under less severe operating conditions, without involving high hydrogen pressures [42,43]. In this procedure, aromatic sulfides recalcitrant to traditional hydrodesulfurization treatments, such as dibenzothiophene (DBT), are oxidized, in a two-steps reaction, to the corresponding sulfoxide and then to the sulfone. Several studies described the use of catalytic systems involving the use of d^0 transition metals (Mo/W heteropolyanions or peroxometals associated to suitable surfactants, to obtain water-in-oil emulsions or ionic liquid phases [44-46], titania supported on silica[47], methyltrioxorhenium supported onto resins [48]) and H_2O_2, leading to deep desulfurization under mild conditions (ranging from room temperature to 80°C) in reaction times ranging from 30 min to few hours.

As a model fuel, we have used *n*-octane, while the oxoclusters are dissolved or dispersed in an extracting CH_3CN phase. In such conditions, DBT dissolves in equimolar amounts into *n*-octane and CH_3CN, and its oxidation products, being less soluble, are almost completely extracted into the most polar phase [20,49,50] (see reaction schemes in Fig. S6). Reactions were performed at T=65°C, in the presence of excess H_2O_2 (3.5 equivs). In Table 2 are reported the reaction yields, calculated with respect to the organic substrate (after 3 and 24 h), initial reaction rates (calculated at <30% substrate conversion), and the selectivities observed at 24 h.

Concerning polymer-free reactions, (entries 2-5 in Table 2), data show that the oxoclusters with lower nuclearity display a higher initial reactivity, with yields higher than 40% after 3h and a marked selectivity for sulfoxide oxidation. Hf_4 appears to be the most efficient one, with >70% yield after 24 h and 91% selectivity for the most oxidized product ($DBTO_2$). Due to the different structure and ligand set, leading to lower hydrolytic stability, Zr_{12} results the least reactive and shows a decreased tendency for sulfoxide oxidation (with <50% $DBTO_2$)[12].

Table 2. Oxidation of DBT by H_2O_2 activated by Zr/Hf oxoclusters.[a]

#	Catalyst	Yield % 3 h	Yield % 24 h	R_0 (μmol L^{-1} s^{-1})	Selectivity $SO:SO_2$[b]
1[c]	-	1	3	-	100:0
2	Zr_4	49	60	0.65	17:83
3	Zr_6	47	52	0.51	28:72
4	Zr_{12}	20	34	0.13	53:47
5	Hf_4	40	73	0.42	9:91
6	Zr_4MMA50T	44	84	0.64	5:95
7	Zr_6MMA50T	53	66	0.84	4:96
8	Zr_{12}MMA50T	25	31	0.36	21:79
9	Hf_4MMA50T	41	89	0.33	6:94
10	Zr_4MMA100T	43	81	0.41	11:89
11	Zr_6MMA100T	43	72	0.72	6:94
12	Zr_{12}MMA100T	29	43	0.21	15:85

[a] Reaction conditions: 1 mL *n*-octane containing 0.01 M DBT, 1 mL CH_3CN containing 0.035 M H_2O_2 (added as 30% aqueous solution) and 15% mol catalyst, T=65°C. [b] DBT is equally distributed in both phases, while DBTO and $DBTO_2$ are completely extracted in CH_3CN; [c] blank reaction without oxoclusters. The addition of methacrylic acid gave analogue results.

Fig. 3a reports the kinetic behavior observed for Zr_4. As for the other homogeneous catalysts (Fig. S7-S17), the kinetic profile is characterized by a steady state regime for the intermediate product, followed by a plateau region. Indeed, due the concurrent oxidant decomposition, the reactions level-off after an initial burst of reactivity.

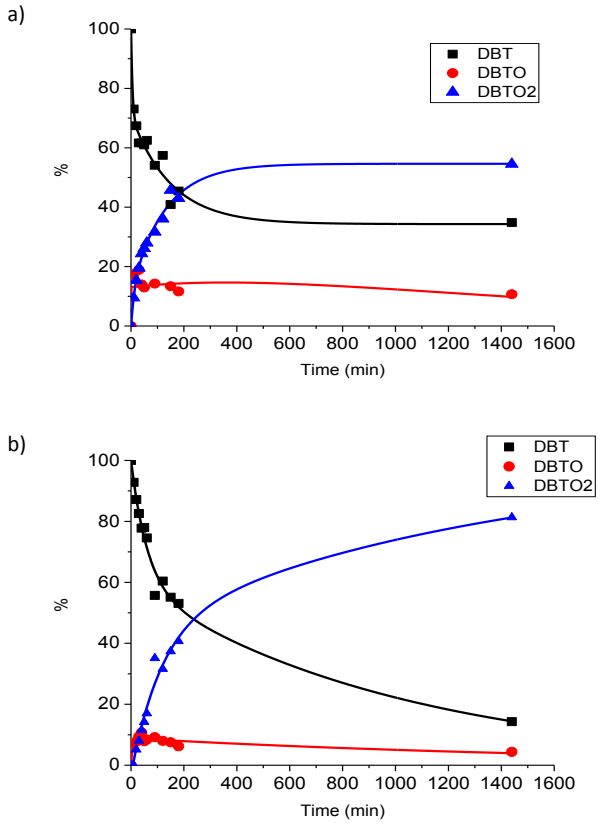

Fig. 3. Kinetic profiles for the oxidation of DBT by H_2O_2 in the presence of (a) Zr_4 and (b) Zr_4MMA50T. DBT concentration has been calculated as the total amount, dissolved both in *n*-octane and in acetonitrile. DBTO and $DBTO_2$ concentrations refer to the acetonitrile phase.

The heterogeneous catalytic tests (entries 6-12 in Table 2) were performed by using grinded polymers. The data highlight a better performance for all polymeric formulations, which retain the initial reactivity observed in homogeneous solution, without showing deactivation at longer reaction time. For example, Zr_4MMA50T reaches 84% yield (vs 60% in homogenous conditions), while Hf_4MMA50T yield rises to 89% (vs 73% in homogenous conditions). The higher reactivity for the embedded oxoclusters is likely due to the enhanced hydrolytic stability of the oxoclusters, coupled with an advantageous enrichment of the substrates (DBT, DBTO) within the polymeric matrix, which favours the conversion to $DBTO_2$ [20]. In addition, only a minor H_2O_2 decomposition is observed in such conditions.

Figure 3b reports the kinetic profile obtained in the presence of Zr_4MMA50T, which displays the best performances, in terms of initial reaction rate and selectivity, among the hybrid materials. The smaller improvements observed for Zr_{12}-based copolymers are likely attributed to the lower incorporation efficiency of this sterically hindered oxocluster in the polymer backbone, as evidenced by swelling experiments and ^{13}C NMR quantitative data.

Despite the much higher swelling degree (Table 1), the hybrids with a oxocluster:MMA molar ratio of 1:100 (100T) display only a minor difference in reactivity with respect to 50T ones. In addition, selectivity towards $DBTO_2$ is decreased, and a parallel unproductive H_2O_2 consumption is observed. This can be due to a lower accessibility to the oxoclusters, as well as to H_2O_2 scavenging by the higher amount of unreacted MMA double bonds.

Porous polymers have been finally prepared, upon addition of a mixture of porogenic solvents (1,4-butandiol and 2-propanol) to the polymerization reaction. In this case, despite the higher accessibility of the oxoclusters, resulting from higher surface area, the reaction efficiency is lower (<42% conversion in 24h). On the other hand, as confirmed by the identical reaction rate observed at different experimental stirring speed (500 or 1000 rpm), the reaction rate seems to be not limited by the diffusion of the reactants within the polymer matrix.

This outcomes highlight the key role of an optimal oxocluster distribution/cross-linking to avoid undesired reactions involving the oxoclusters and the oxidant.

3.3. Recovery, reuse and structural assessment of the hybrid materials

To confirm the positive effects of the polymeric matrix against possible changes in both structure and/or composition of the catalytic materials, we have performed further analyses on the hybrid materials after catalysis. It should be underlined that these changes could be induced by degradation phenomena ascribed either to the polymer matrix or rather to the oxocluster: (i) leaching of the oxocluster from the polymer matrix; (ii) hydrolysis/condensation or oxidation reactions of the oxoclusters; (iii) oxidation of the polymer matrix. Whereas the first possible degradation phenomenon is less probable, being the oxocluster covalently linked to the matrix, the others have deserved a closer insight. The studies were focused on Zr_4MMA50T, which exhibits the best catalytic performances. The stability of the oxocluster was investigated by XAS, which has been already assessed as a powerful tool to study the stability of inorganic building blocks in hybrid materials [51], and to provide details on the local chemical environment of the metal species (in this case Zr). In particular, this technique was useful to provide preliminary insights on the formation of peroxospecies when the pure oxocluster is incubated with a strong H_2O_2 excess [12]. Fig. 4 reports the k^3-weighted EXAFS functions (a) and the corresponding Fourier transforms (b, phase-shifted) for Zr_4 and the 1:50 hybrid before (Zr_4MMA50T) and after catalysis (Zr_4MMA50A). As it can be noted, the EXAFS functions do not present significant variations among the different samples, with only a minor difference at about 7 $Å^{-1}$ between the pure oxocluster and the two hybrids. Such minor changes are more evident in the Fourier transforms, in particular in the first shell range (1.3-2.7 Å). This first shell signal is divided in two peaks, representing the two Zr-O distances expected (see Table 3), and shows only a slight decrease in the second band intensity (at 2.25 Å) for the hybrid Zr_4MMA50T materials, with respect to the pure Zr_4. The retention of all spectral features evidences that when the oxocluster is embedded in the polymeric matrix only minor structural changes occur in its core (SS-NMR highlighted a certain disorder affecting the methacrylate groups). The signal at 3.5 Å, corresponding to a Zr-Zr distance, does not show any variation and suggests that the oxocluster retains its structure during catalysis and it is not decomposed. These findings are further confirmed by the fitting of the experimental spectra with theoretical models based on the crystal structure, as reported in Table 3. The modeling does not evidence any significant change between the different samples, thus confirming the stability of the cluster during the catalytic process.

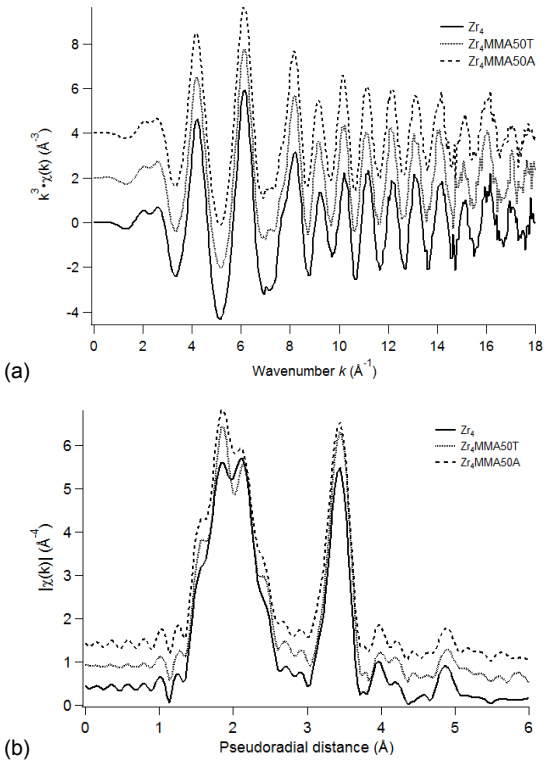

Fig. 4. a) k^3-weighted EXAFS functions (at Zr K-edge) and b) corresponding Fourier transforms for Zr_4 (solid line), Zr_4MMA50T (dotted) and Zr_4MMA50A (dashed).

Table 3. Numeric results from fitting the experimental EXAFS spectra with theoretical model Zr_4.

Sample	Abs-Bs[a]	Coordination number	R (Å) [b]	σ^2 (Å^2) [c]
Zr_4 (XRD)[24]	Zr-O	4.5	2.14	-
	Zr-O	3.0	2.23	-
	Zr-Zr	2.5	3.59	-
Zr_4	Zr-O	4.5±0.7	2.12±0.02	0.004±0.001
	Zr-O	6.2±0.9	2.25±0.02	0.004±0.001
	Zr-Zr	2.8±0.8	3.52±0.01	0.005±0.001
Zr_4MM50T	Zr-O	4.8±0.6	2.11±0.02	0.004±0.001
	Zr-O	6.0±0.7	2.25±0.01	0.004±0.001
	Zr-Zr	3.8±0.9	3.52±0.01	0.006±0.001
Zr_4MM50A	Zr-O	5.3±0.7	2.12±0.02	0.005±0.001
	Zr-O	6.1±0.7	2.26±0.01	0.005±0.001
	Zr-Zr	3.4±0.8	3.53±0.01	0.005±0.001

[a] Abs=absorber atom, Bs=backscattering atom [b] Distance Abs-Bs [c] Debye-Waller factor

A further insight into the microstructure of the hybrid materials the oxocluster distribution in the polymer matrix, as well as the effect of the catalytic process on the microstructure was pursued by Small Angle X-ray Scattering (SAXS). Fig. 5 shows SAXS data of four samples: Zr_4MMA50T before and after catalysis (Zr_4MMA50A), Zr_6MMA50T and Zr_4MMA50P (with porogenic solvents). In a log-log-plot the SAXS data exhibit an almost perfect Porod law, i.e. they obey $I(s) \propto 1/s^4$ at larger values of the modulus of the scattering vector s, indicating the presence of objects (oxoclusters) possessing a significantly different electron density than the surrounding matrix.

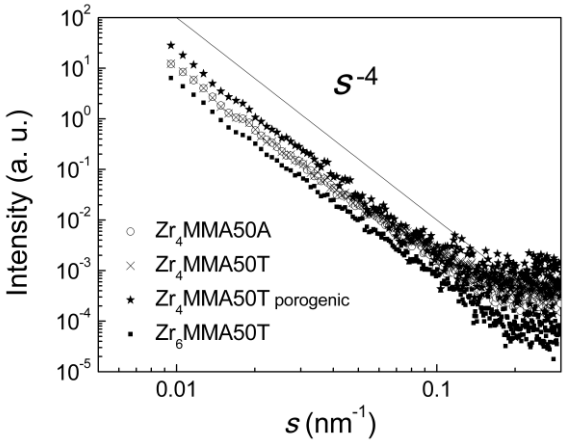

Fig. 5. SAXS data collected for various 1:50 hybrids.

The fact that no maxima in I(s) are observable indicates the lack of long-range and short-range order and thus are in conformity with a homogeneous statistic distribution of the oxoclusters or small aggregates of oxoclusters within the polymeric matrix. However, the absence of maxima and the SAXS data measured at quite small values of s allow for the analysis by the Guinier law $I(s) \propto \exp(-(4\pi^2 s^2 R_g^2)/3)$ (where R_g is the radius of gyration), being applicable as asymptotic behavior in the region of small s values. Indeed, the SAXS data of the four samples shown in Fig. 5 fulfill the Guinier law at small s, and for all samples an average value of R_g ca. 10 nm can be extracted from fitting the SAXS data at small s. This value seems to be quite large at a first glance, but is in conformity with a diameter of ca. 2 nm, i.e. in the range expected for the oxoclusters. Thus, a value of R_g = 10 nm indicates the formation of small aggregates of several oxoclusters. Interestingly, the SAXS data are almost identical for all of these samples. Thus, the cluster size does not change during the catalytic reaction, i.e. these results further confirm that the oxoclusters remain chemically intact, which is also in agreement with XAS data.

Concerning FT-IR data of Zr_6MMA50T, the more striking difference pointed out between the materials before and after the catalysis is the decrease of the intensity of the band due to double bonds, which is ascribed to their oxidation in the presence of H_2O_2 (Fig. S18). On the other hand, the rRaman spectra of Zr_6MMA50T, collected before and after the reaction, do not display any change, thus confirming its stability under oxidative conditions. Nevertheless, the rRaman spectra collected after addition of H_2O_2, in acetonitrile, display minor changes between 800 and 900 cm^{-1}, i.e. the region where peroxometal bonds give a resonance signal (Fig. S19).

The ^{13}C SS-NMR spectra of Zr_4MMA50T, Zr_6MMA50T and Zr_{12}MMA50T recovered after the catalysis are shown in Fig. 2 They can be collectively commented since the same effects are observed. Firstly, it can be noticed that the signals of PMMA are substantially unchanged indicating that the catalytic process does not strongly alter the polymeric backbone. The most evident effect is the appearance of four relatively narrow peaks at 15.0, 23.0, 29.8, 36.2 ppm (the first two superimposed to the broad

methyl signal) and one at about 1.2 ppm, which must be ascribed to residual octane and acetonitrile, respectively. No signals due to DBT or to its oxidation products were observed. Comparing the spectra before and after the catalysis it is also possible to observe a slight intensity increase of the PMMA signals between 40 and 60 ppm with respect to the other signals, which could be tentatively ascribed to a slight stiffening of the polymer main chain, and a slight decrease of the signals due to the olefinic carbon atoms, in agreement with FT-IR outcomes.

As far as the morphology of the hybrids is concerned, the specific surface area of the materials (Zr_4MMA50T), measured by BET analysis, remains practically unchanged, from 2.1 m^2g^{-1} before the catalysis to 1.9 m^2g^{-1} after the catalysis. The morphology of the hybrid materials was also investigated by SEM. While the samples show a smooth surface (interrupted only by cracks due to drying process), the presence of the porogenic solvents (Fig.S20) induces an increased roughness of the hybrid interface, and pores in the order of hundreds of nm diameter can be observed.

To evaluate the retention of the catalytic activity, the reaction mixture containing Zr_4MMA50T was recharged (three times, at t=24 h intervals) with further DBT and with H_2O_2. The second run showed a 50% decrease of the catalytic efficiency, in terms of total sulfur removal, these performances were found to stabilize during next runs (Fig. S21). On the other hand, much better performances were obtained after removal and washing of the catalyst from the reaction mixture, in order to remove the adsorbed products. In this case, very similar performances were observed, with the same initial rate (R_0=3.1x10^{-7} mol L^{-1} s^{-1}), 80% yield in 24 h and 1:99 SO:SO_2 selectivity (Fig. S22). The absence of catalyst leaching from the bulk polymer was then assessed by removing the hybrid material from the reaction mixture after two hours of reaction. Although some DBTO can still form from the uncatalyzed oxidation (see Table 2), the observation of a constant concentration of $DBTO_2$ is in agreement with the absence of active metal species in solution. Accordingly, a negligible amount of Zr (<250 ppb) was observed by ICP-MS in both filtrated phases.

Such performances confirm the positive effects of the polymeric matrix, which, beside allowing an easy recycling, improves the stability and the catalytic efficiency.

4. Conclusions

A set of novel polymethyl methacrylate polymers, covalently reinforced by polymerizable Zr/Hf oxoclusters has been prepared and used for the first time as stable heterogeneous catalysts.

By a combined investigation, based on FT-IR and ^{13}C SS-NMR spectroscopies, it was possible to verify the structure of the oxoclusters and of the hybrids, thus revealing and quantifying a fraction of unreacted double bonds. SS-NMR data also evidenced how this fraction is higher for Zr_{12}-based hybrids, due to the elevated steric hindrance characterizing this cluster. Accordingly, the lower cross-linking efficiency for Zr_{12}-based hybrids was also confirmed by swelling experiments. Thermogravimetry highlighted an increased thermal stability for hybrid materials, compared to pristine PMMA.

The catalytic efficiency of the oxoclusters was demonstrated in the sulfoxidation of dibenzothiophene (DBT) by H_2O_2, in a biphasic (*n*-octane/CH_3CN) system, as an example of sustainable oxydesulfurization (ODS), where sulfur content can be reduced from 300 to 25-65 ppm in 24 h at 65°C. The heterogeneous catalysts show an enhanced activity, in terms of reaction yield and selectivity, with respect to the soluble oxoclusters, pointing to a major role of the polymeric matrix in shaping a suitable environment for implementing catalyst stability and reaction selectivity. The comparison between FT-IR, rRaman and SS-NMR spectra recorded before and after the catalysis shows indeed a substantial stability of the hybrids. The stability of the clusters throughout the catalytic reaction was also evidenced by XAS experiments. Neither the XANES nor EXAFS regions showed any significant difference after catalysis, being the spectral features of the best performing material very similar to those of pure Zr_4 cluster. Thanks to this stability, Zr_4MMA50T could be recovered and recycled with no loss of activity.

Despite the lower reactivity, with respect to recent literature reports on ODS process [44-50], our results represent a fundamental step further toward the development of a novel class of metal oxoclusters-based heterogeneous catalysts. On the other hand, the possibility to modify the properties of the hybrids, depending on the oxocluster nature and on the addition of suitable additives was demonstrated. Further investigations are required to optimize the morphology and the affinity towards the substrates, while addressing incomplete cross-linking and solubility issues.

Acknowledgments

Dr. Ingrid Zenke (Max-Planck Institute of Colloids and Interfaces) is thanked for performing the SAXS measurements, Dr. Roberta Saini (University of Padova) is acknowledged for TGA-DSC measurements and Dr. Denis Badocco (University of Padova) is acknowledged for ICP-MS measurements. The Italian Foreign Affairs Ministry (Ministero degli Affari Esteri, MAE, Italy) and the National Research Council (CNR, Italy) are gratefully acknowledged for the financial support of this work in the framework of the "Progetto Grande Rilevanza Italia-Slovenia 2013". The University of Padova, the Italian Consortium INSTM are acknowledged for providing money and equipment. We would like to thank Dr. G. Aquilanti and Dr. L. Olivi for their support during EXAFS measurements and the European Community for financial support in activities under the EU Calipso Programme. The research leading to these results has received funding from the European Community's Seventh Framework Program (FP7/2007-2013) under grant agreement n° 226716. A.S and M.C. acknowledge the financial support from Fondazione Cariparo (Progetto Dottorati di Ricerca PARO118894/11).

References and notes

[1] Schubert U., *Macromol. Symp.* **2008**, *267*, 1–8.
[2] Schubert U., *Chem. Soc. Rev.* **2011**, *40*, 575–582.
[3] Albinati A., Faccini F., Gross S., Kickelbick G., Rizzato S., Venzo A., *Inorg. Chem.* **2007**, *46*, 3459–3466.
[4] Lane B.S., Burgess K., *Chem. Rev.* **2003**, *103*, 2457–2473.
[5] Arends I.W.C.E., Conte V., Licini G., in *Innov. Catal. Org. Synth. Oxidation, Hydrog. C-X Bond Form. React.*, **2012**, pp. 77–102.
[6] Mal S.S., Nsouli N.H., Carraro M., Sartorel A., Scorrano G., Oelrich H., Walder L., Bonchio M., Kortz U., *Inorg. Chem.* **2010**, *49*, 7–9.
[7] Jahier C., Mal S.S., Kortz U., Nlate S., *Eur. J. Inorg. Chem.* **2010**, 1559–1566.
[8] Carraro M., Nsouli N.H., Oelrich H., Sartorel A., Sorarù A., Mal S.S., Scorrano G., Walder L., Kortz U., M. Bonchio, *Chem. - A Eur. J.* **2011**, *17*, 8371–8378.
[9] Li D., Han H., Wang Y., Wang X., Li Y., Wang E., *Eur. J. Inorg. Chem.* **2013**, 1926–1934.
[10] Kholdeeva O.A., Maksimovskaya R.I., *J. Mol. Catal. A Chem.* **2007**, *262*, 7–24.

[11] Al-Kadamany G., Mal S.S., Milev B., Donoeva B.G., Maksimovskaya R. I., Kholdeeva O.A., Kortz U., *Chem. - A Eur. J.* **2010**, *16*, 11797–11800.
[12] Faccioli F., Bauer M., Pedron D., Sorarù A., Carraro M., Gross S., *Eur. J. Inorg. Chem.* **2015**, *2015*, 210–225.
[13] Bahrami K., *Tetrahedron Lett.* **2006**, *47*, 2009–2012.
[14] Gross S., *J. Mater. Chem.* **2011**, *21*, 15853-15861.
[15] Carraro M., Gross S., *Materials.* **2014**, *7*, 3956–3989.
[16] Kholdeeva O.A., Maksimchuk N.V., Maksimov G.M., *Catal. Today*, **2010**, 107–113.
[17] Biffis A., Zecca M., Basato M., *J. Mol. Catal. A Chem.* **2001**, *173*, 249–274.
[18] Bonchio M., Carraro M., Scorrano G., Fontananova E., Drioli E., *Adv. Synth. Catal.* **2003**, *345*, 1119–1126.
[19] Carraro M., Gardan M., Scorrano G., Drioli E., Fontananova E., Bonchio M., *Chem. Commun.*. **2006**, 4533–4535.
[20] Carraro M., Fiorani G., Mognon L., Caneva F., Gardan M., Maccato C., Bonchio M., *Chem. Eur. J.* **2012**, *18*, 13195–13202.
[21] Bonchio M., Carraro M., Gardan M., Scorrano G., Drioli E., Fontananova E., in *Top. Catal.*, **2006**, pp. 133–140.
[22] Campos-Martin J.M., Capel-Sanchez M.C., Fierro J.L. G., *Green Chem.* **2004**, *6*, 557–562.
[23] Al-Shahrani F., Xiao T., Llewellyn S.A., Barri S., Jiang Z., Shi H., Martinie G., Green M.L.H., *Appl. Catal. B Environ.* **2007**, *73*, 311–316.
[24] Ballistreri F.P., Tomaselli G.A., Rosa V., Toscano M., Conte V., Di Furid F., **1991**, 6209–6212.
[25] Gross S., Kickelbick G., Puchberger M., Schubert U., *Monatshefte fur Chemie* **2003**, *134*, 1053–1063.
[26] Trimmel G., Gross S.,. Kickelbick G, Schubert U., in *Appl. Organomet. Chem.*, **2001**, pp. 401–406.
[27] Kickelbick G., Wiede P., Schubert U., *Inorganica Chim. Acta* **1999**, *284*, 1–7.
[28] Puchberger M., Kogler F.R., Jupa M., Gross S., Fric H., Kickelbick G., Schubert U., *Eur. J. Inorg. Chem.* **2006**, *2006*, 3283–3293.
[29] Trimmel G., Fratzl P., Schubert U., *Chem. Mater.* **2000**, *12*, 602–604.
[30] Ravel B., Newville M., *J. Synchrotron Radiat.* **2005**, *12*, 537–541.
[31] Allen G., Bevington J.C., in *Compr. Polym. Sci. Suppl.*, Pergamon Press, **1989**.
[32] Elias H.G., Makromoleküle: Struktur, Eigenschaften, Synthesen, Stoffe, Hüthig & Wepf, Basel, **1990**.
[33] Mayer C.R., Thouvenot R., Lalot T., *Chem. Mater.* **2000**, *12*, 257–260.
[34] Graziola F., Girardi F., Bauer M., Di Maggio R., Rovezzi M., Bertagnolli H., Sada C., Rossetto G., Gross S., *Polymer.* **2008**, *49*, 4332–4343.
[35] Nakamoto K., Infrared and Raman Spectra of Inorganic and Coordination Compounds: Part B: Applications in Coordination, Organometallic, and Bioinorganic Chemistry, **2008**.
[36] Kogler F.R., Schubert U., *Polymer.* **2007**, *48*, 4990–4995.
[37] Walther P., Puchberger M., Kogler F.R., Schwarz K., Schubert U., *Phys. Chem. Chem. Phys.* **2009**, *11*, 3640–3647.
[38] Schaefer J., Stejskal E.O., Buchdahl R., *J. Macromol. Sci. - Phys.* **1977**, *B13*, 384–405.
[39] Eijkelenboom A.P.A.M., Maas W.E.J.R., Veeman W.S., Buning G.H.W., Vankan J.M.J., *Macromolecules* **1992**, *25*, 4511–4518.
[40] Noyori R., Aoki M., Sato K., *Chem. Commun.* **2003**, 1977–1986.
[41] Haw K.G., Bakar W.A.W.A., Ali R., Chong J.F., Kadir A.A.A., *Fuel Process. Technol.* **2010**, *91*, 1105–1112.
[42] Zhu W., Li H., Jiang X., Yan Y., Lu J., He L., Xia J., *Green Chem.* **2008**, *10*, 641-646.
[43] Jiang Y., Zhu W., Li H., Yin S., Liu H., Xie Q., *ChemSusChem* **2011**, *4*, 399–403.
[44] Sachdeva T.O., Pant K.K., *Fuel Process. Technol.* **2010**, *91*, 1133–1138.
[45] Li C., Jiang Z., Gao J., Yang Y., Tian F., Sun F., Sun X., Ying P., *Chem. Eur. J.* **2004**, *10*, 2277–2280.
[46] Zhu W., Zhu G., Li H., Chao Y., Du D., Wang Q., Zhao Z., *Fuel Process. Technol.* **2013**, *106*, 70–76.
[47] Frailea J. M., Gil C., Mayoral J. A., Muel B., Roldán L., Vispe E., Calderón S., Puente F., *Appl. Catal. B: Environ.* **2016**, *180*, 680–686.
[48] Di Giuseppe A., Crucianelli M., De Angelis F., Crestini C., Saladino R., *Appl. Catal. B: Environ.* **2009**, *89*, 239–245.
[49] Yazu K., Yamamoto Y., Furuya T., Miki K., Ukegawa K., *Energy Fuels* **2001**, *15*, 1535–1536.
[50] Capel-Sanchez M.C., Perez-Presas P., Campos-Martin J.M., Fierro J.L.G., *Catal. Today* **2010**, *157*, 390–396.
[51] Gross S., Bauer M., *Adv. Funct. Mater.* **2010**, *20*, 4026–4047.

Graphical Abstract

Engineering of oxoclusters-reinforced polymeric materials with application as heterogeneous oxydesulfurization catalysts

Leave this area blank for abstract info.

Marilisa Vigolo, Silvia Borsacchi, Antonio Sorarù, Marco Geppi, Bernd Smarsly, Paolo Dolcet, Silvia Rizzato, Mauro Carraro*, Silvia Gross*

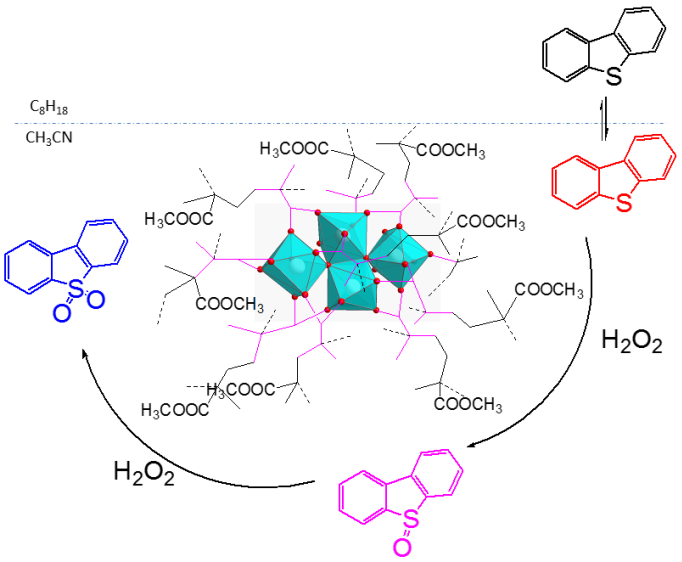

Highlights

- Polyacrylate polymers were reinforced upon cross-linking with Zr/Hf oxoclusters
- The hybrid polymers were used for the first time as catalysts for H_2O_2 activation
- The hybrid polymers enable the heterogeneous oxydesulfurization of a model fuel
- The polymeric environment fosters the oxidation of dibenzothiophene to its sulfone
- SS-NMR, XAS, SAXS demonstrate the high stability of the cross-linked oxoclusters

Supplementary Material

Click here to download Supplementary Material: ACBE_SM_Carraro_Gross_revised.docx

Applied Catalysis B: Environmental
journal homepage: www.elsevier.com

Engineering of oxoclusters - reinforced polymeric materials with application as heterogeneous oxydesulfurization catalysts

Marilisa Vigolo[a,b], Silvia Borsacchi[b,c], Antonio Sorarù[a], Marco Geppi[b,c,d], Bernd Smarsly[e], Paolo Dolcet[a,b,f], Silvia Rizzato[g], Mauro Carraro* [a, h], Silvia Gross*[a,b,f]

[a] *Dipartimento di Scienze Chimiche, Università degli Studi di Padova, via Marzolo, 1, I-35131, Padova, Italy*
[b] *INSTM, Consorzio Interuniversitario per la Scienza e Tecnologia dei Materiali, via Giusti 9, 50121, Firenze, Italy*
[c] *Istituto di Chimica dei Composti Organometallici del Consiglio Nazionale delle Ricerche, Area della Ricerca di Pisa-S. Cataldo, Via G. Moruzzi 1, 56124 Pisa, Italy*
[d] *Dipartimento di Chimica e Chimica Industriale, Università di Pisa, via G. Moruzzi 13, 56124 Pisa, Italy*
[e] *P hysikalisch-Chemisches Institut, Justus-Liebig-Universität Giessen, Heinrich-Buff-Ring 58, D-35392 Giessen, Germany*
[f] *Istituto per l'Energetica e le Interfasi, IENI-CNR via Marzolo, 1, I-35131, Padova, Italy*
[g] *Dipartimento di Chimica, Università degli Studi di Milano, via Golgi, 9, I-20133, Milano, Italy*
[h] *Istituto per la Tecnologia delle Membrane, ITM-CNR via Marzolo, 1, I-35131, Padova, Italy*
* *E-mail; mauro.carraro@unipd.it; silvia.gross@unipd.it*

Dedicated to the memory of our friend and colleague Prof. Alessandro Bagno, Full Professor of Organic Chemistry at the University of Padova, unexpectedly and prematurely passed away on 23.3.2015

ARTICLE INFO

Article history:
Received
Received in revised form
Accepted
Available online

Keywords:
oxoclusters
hybrid materials
peroxides
DBT oxidation
Solid State NMR

ABSTRACT

In this paper we report the first example of hybrid materials based on polymethlymethacrylate (PMMA) matrices covalently reinforced by $M_yO_x(OH)_w(O(O)CR)_z$ oxoclusters (M=Zr or Hf), used as heterogeneous catalytic systems for hydrogen peroxide activation. The resulting hybrids were used to catalyze the oxidation of dibenzothiophene (DBT) to the corresponding sulfoxide (DBTO) and sulfone ($DBTO_2$), in order to demonstrate their potential application for the oxydesulfurization (ODS) of a fuel. Thanks to catalyst confinement and to the higher affinity of the polymeric matrix towards polar substrates, the heterogeneous set-up displays improved performances with respect to the corresponding homogeneous systems. At 65°C, a DBT conversion higher than 84% was obtained in 24 h, with a >94% selectivity for $DBTO_2$. The stability of the hybrid materials under catalytic conditions was successfully assessed by a combined spectroscopic approach, based on FT-IR, resonance Raman, Solid State Nuclear Magnetic Resonance, X-ray Absorption and Small Angle X-ray scattering measurements.

1. Introduction

Oxoclusters of early transition metals are a versatile class of polynuclear compounds built up of a limited number of 3-5 groups metal atoms, such as Ti^{IV}, Zr^{IV}, Hf^{IV} or Nb^{V}, linked by oxygen bridges and coordinated by organic ligands [1,2]. These compounds are globally neutral and discrete species with general formula $M_yO_x(OH)_w(O(O)CR)_z$, where typically organic carboxylates act as bidentate ligands. They can display different nuclearities (i.e. number of constituent metal atoms, y = 2–12), coordination number of the metal atoms (varying between 6 and 9) and connectivity modes (corner, edge or face sharing of polyhedral units). In some cases they also involve an alkaline earth (e.g. Ba, Mg) metal [3].

Since these oxoclusters are characterized by the presence of early transition metals in their highest oxidation state, they are appealing candidates as catalysts for peroxide activation [4,5]. Moreover, Zr and Hf-based multimetallic complexes have been reported to activate hydrogen peroxide, promoting the oxidation of different substrates (sulfides and sulfoxides, alcohols) both in water and in organic solvents [6–11]. As far as zirconium-based oxoclusters are concerned, we have recently evidenced the possibility to use two different complexes to activate hydrogen peroxide and oxidize organic substrates [12]. In such preliminary study, the oxidation of methyl *p*-tolylsulfide to the corresponding sulfoxide and sulfone was chosen as model reaction, showing an interesting reactivity towards sulfoxide oxidation [13]. However, despite the encouraging results, the hydrolytic stability of such oxoclusters is too low to allow a practical application in homogeneous catalysis, since they easily rearrange and precipitate from the reaction mixture.

Owing to the possibility to use oxoclusters as building blocks for the synthesis of different typologies of hybrid materials [14] with enhanced functional (e.g. dielectric, magnetic etc.) and

structural (thermal, mechanical) properties [15], we have devised novel heterogeneous systems based on the covalent immobilization of Zr and Hf oxoclusters into a polymeric matrix.

The protection of a catalytically active system by embedding/anchoring it within a matrix is an underlying and widely used strategy in heterogeneous catalysis [16]. Within this scenario, the preparation of hybrid materials through the integration of the multimetallic catalytic active species into a polymeric matrix is a fertile field of research [17–20]. Indeed, this strategy offers interesting perspectives for devising continuous flow processes, where the polymer may contribute to improve the reaction selectivity and/or enable process intensification, by coupling catalysis and separation technologies [20,21]. Nevertheless, to the best of our knowledge, the hybrid materials here described are the first example of heterogeneous catalysts based on the covalent immobilization of oxoclusters. Not only the covalent bonds endow the final material with enhanced stability, but also prevent phases separation inside the polymer matrix and leaching.

In this framework, different acrylate copolymers were prepared by changing the nature of the oxocluster as well as the oxocluster/monomer molar ratio, which in turn, *inter alia*, affect the cross-linking degree of the resulting hybrid. The effectiveness of the hybrid materials as heterogeneous catalysts was evaluated in the oxidation of an aromatic sulfide by H_2O_2, in a biphasic *n*-octane/acetonitrile system, as an example of sustainable fuel desulfurization process [22,23]. In particular, we exploited the oxocluster reactivity to perform the oxidation of dibenzothiophene (DBT), dissolved in *n*-octane, to the corresponding sulfoxide (DBTO) and sulfone ($DBTO_2$), whereby the oxidized products can be easily extracted by the polar solvent [20]. Thanks to the enhanced affinity of the polymeric matrix toward polar substrates and solvents, the heterogeneous set-up shows better performances than the corresponding homogeneous systems. Furthermore, the heterogeneous catalysts can be recovered and reused. FT-IR, resonance Raman, Solid State Nuclear Magnetic Resonance (SS-NMR), X-ray Absorption (XAS), and Small Angle X-ray scattering measurements (SAXS) highlighted, indeed, that the hybrids are endowed with appreciable stability even after catalytic turnover.

2. Experimental

2.1. Materials and chemicals

Zirconium butoxide ($Zr(O^nBu)_4$, 80% wt in *n*-butanol), zirconium propoxide ($Zr(O^nPr)_4$) 70% wt in *n*-propanol), vinylacetic acid, dibenzothiophene (DBT), dibenzothiophene sulfone ($DBTO_2$), hydrogen peroxide (30% wt in water) were all purchased from Sigma-Aldrich and used as received. Hafnium butoxide ($Hf(O^nBu)_4$, 95% wt in *n*-butanol) was supplied by ABCR. Methacrylic acid 99%, and methymethacrylate, purchased from Sigma-Aldrich, were filtered on neutral alumina to remove the inhibitor. All the chemicals were stored under argon, while the solvents were additionally stored on molecular sieves. Dibenzothiophene sulfoxide (DBTO) was synthesized following a literature procedure [24]. Oxoclusters $M_4O_2(O(O)CC(CH_3)=CH_2)_{12}$ (Hf_4, with M=Hf) [25] or (Zr_4, with M=Zr) [26], $Zr_6(OH)_4O_4(O(O)CC(CH_3)=CH_2)_{12}$ (Zr_6) [27], $[Zr_6O_4(OH)_4(O(O)CCH_2CH=CH_2)_{12}]_2\cdot 6CH_2=CHCH_2C(O)OH$ (Zr_{12}) [28], were synthesized under argon, using standard Schlenk techniques, according to literature procedures. The structure of all oxoclusters was confirmed by measuring the unit cell dimensions on a number of different single crystals by diffraction technique. Moreover, the nature of the bulk precipitate formed by a mixture of single crystals and an apparently amorphous solid has been investigated by X-ray powder diffraction techniques, by comparison with the spectra simulated from the single crystal data that has confirmed the purity of the products.

2.2. Hybrid materials syntheses

The hybrid materials were prepared by implementing a known procedure [29]. In a typical polymerization, a weighed amount (0.7 g, moles amount depending on the oxocluster) of oxocluster was dissolved in methyl methacrylate (3-12 g), so to achieve oxocluster : MMA molar ratios of 1:50, 1:100, and 1:200. The thermoinitiator benzoylperoxide (BPO) (3% wt. with respect to the monomer) was finally added to the suspension and the reaction mixture was heated at 80°C for 1 h. Glassy monolithic materials were thus obtained. Samples were labeled as M_xMMAnT with M=Zr and x=4, 6 or 12, or M=Hf and x=4, n (molar ratio) = 50, 100 or 200, while T stands for thermal polymerization. Reference PMMA (poly methyl methacrylate) was prepared by using the same procedure, without adding the oxocluster. Porogenic solvents (1,4-butandiol and 2-propanol, 1:2 v/v) were added to the reaction mixture to produce porous polymers. In this latter case, samples were labeled as M_xMMAnP.

2.3. Solid State NMR measurements

^{13}C SS-NMR spectra were recorded on a Varian InfinityPlus 400 spectrometer, working at a Larmor frequency of 400.02 MHz and 100.59 MHz for proton and carbon nuclei, respectively, using a 7.5 mm probehead with a 90° 1H pulse duration of 5 μs. ^{13}C Cross Polarization-Magic Angle Spinning (CP-MAS) spectra were recorded with high-power decoupling from ^1H nuclei, spinning the samples at a MAS frequency between 5 and 6 kHz (depending on the sample), using a contact time of 1 ms, a recycle delay of 5 s and accumulating 10000 transients. The ^{13}C chemical shift scale was calibrated using hexamethylbenzene and TMS as secondary and primary references, respectively. All the spectra were recorded at 25 °C, using air as spinning gas.

2.4. XAS measurements

Synchrotron (Trieste, Italy). A Si(311) double crystal monochromator was used for measurements at the Zr K-edge (17.998 keV). The second monochromator crystal was tilted for optimal harmonic rejection. The spectra were recorded in transmission mode using ionization chambers as detectors. Energy calibration was performed with a Zr metal foil. The solid samples were pressed into self-supporting pellets using cellulose as a binder.

Data evaluation started with background absorption removal from the experimental absorption spectrum by using the automated removal routine found in the Athena software [30]. The threshold energy E_0 was determined as the maximum in the first derivative spectrum. To determine the smooth part of the spectrum, corrected for pre-edge absorption, a piecewise polynomial was used. It was adjusted in such a way that the low-R components of the resulting Fourier transform were minimal. After division of the background–subtracted spectrum by its smooth part, the photon energy was converted to photoelectron wave numbers k. The resulting $\chi(k)$-function was weighted with k^3 and Fourier transformed using a Hanning window function.

Data analysis was performed in k-space on unfiltered data, using the Artemis software [30].

2.5. SAXS measurements

SAXS patterns were recorded employing a Nonius rotating anode generator equipped with a 3 pin-hole setup (installed at Max-Planck-Institute of Colloids and interfaces) providing a wavelength of $\lambda = 0.154$ nm (CuK_α radiation), and using a MAR CCD area-detector. The 2D SAXS patterns were radially averaged, providing 1D SAXS intensity scans as a function of the modulus of the scattering vector $s = 2/\lambda \sin(\theta)$, where 2θ is the scattering angle.

2.6. SEM measurements

Scanning Electron Microscopy measurements were performed using a field emission SEM, Zeiss SUPRA 40VP equipped with an EDXS system (Oxford INCA), by using a primary beam acceleration voltage of 10 kV.

2.7. FT-IR measurements

Infrared spectra were collected by using a Thermo Quest Nicolet 5700 instrument. Few milligram of oxocluster before and after catalysis were dispersed into KBr pellets.

2.8. Inductively coupled plasma - mass spectrometry (ICP-MS)

An ICP-MS Agilent Technologies 7700 instrument, operating at 1550 W plasma power was used to detect the amount of Zr released in solution. A CEM Discover SP-D microwave reactor was used for the microwave assisted acid (HNO_3+HF 7:1) digestion of the samples. The instrumental operating conditions were as follows: T_{max} = 180 °C, ramp time = 4 min, stop time = 10 min, power = 300 W.

2.9. Raman measurements

Raman spectra were collected by using a Thermo DXR Raman Microscope. A 780 nm laser was used as excitation source, operated at a power of 24 mW.

2.10. Catalytic tests

For the oxidation reactions, the oxocluster (1.5 μmol) was dissolved in CH_3CN (1 ml) and mixed with a *n*-octane solution (1 ml) containing DBT (10 μmol). The biphasic systems were stirred for 5 min before adding H_2O_2 (35 μmol, added as 30% aq. solution). The reactions were performed at 65°C and monitored over 24 h. H_2O_2 consumption was verified by iodinated paper. Samples (20 μL) of both phases were withdrawn at fixed time interval, diluted in a CH_3CN solution, containing 9-fluorenone as chromatographic standard, and treated with supported triphenylphosphine as oxidant quencher. The samples were then filtered on membrane filters (0.45 μm) and analyzed by HPLC, using a Gemini C18 column (Phenomenex) eluted (1 mL min^{-1}) with the following solvent gradient: H_2O/CH_3CN (40:60) for 2 min, 100% CH_3CN at 9 min; the UV detector was set at λ= 220 nm.
In all reactions, the amount of material was established in order to provide the same amount of oxoclusters.

Catalyst stability and its recycling were assessed by (i) recharging the reaction mixture with further aliquots of DBT and H_2O_2, (ii) reusing the recovered catalyst, after centrifugation and washing with acetonitrile, (iii) by checking the residual reactivity of the reaction mixture after removal by filtration of the oxocluster. The recovered catalysts, labeled as M_xMMAnA were analyzed by FTIR, Raman, ^{13}C CP-MAS spectra.
Blank reactions were performed without catalyst as well as by using the methacrylic acid, to exclude the formation of peracids.

2.11. Swellings

The swelling experiments were carried out by simply leaving carefully weighted normalized samples of polymers in ethylacetate and water for 72 hours. Then the percentage weight increase of all the samples was determined and the swelling index (I_{sw}) could be calculated according to [31–33]:
I_{sw} = wet weight- dry weight/dry weight

3. Results and discussion

3.1. Synthesis and characterization of the oxocluster-based organic inorganic hybrid materials.

The hybrid materials were synthesized by implementing a previously published procedure, based on the copolymerization of the methacrylate- or vinylacetate [34] functionalized oxoclusters with methlymethacrylate (MMA) monomers, to give an oxocluster-reinforced polymeric matrix.
In particular, the nature of the oxocluster as well as its molar ratio with respect to the monomers were systematically varied in the preparation of the hybrids, in order to assess their effect on the catalytic properties. In the following Table 1, the prepared samples and their composition are collected.

Table 1. Samples labelling and swelling data.

Sample name	Oxocluster/monomer molar ratio	Swelling[a]
Zr_4MMA50T	1:50	59
Zr_4MMA100T	1:100	100
Zr_4MMA200T	1:200	209
Zr_6MMA50T	1:50	39
Zr_6MMA100T	1:100	54
Zr_6MMA200T	1:200	100
Zr_{12}MMA50T	1:50	56
Zr_{12}MMA100T	1:100	- [b]
Zr_{12}MMA200T	1:200	- [b]
Hf_4MMA50T	1:50	50

[a] Calculated after 72 h in ethylacetate. [b] The material is soluble.

The materials were firstly characterized to confirm the presence of the oxoclusters and to investigate the possible presence of residual double bonds, in order to assess the polymerization degree. Due to the overwhelming contribution of the PMMA matrix, all FT-IR spectra appear very similar each other (See Fig.1), with C=O stretching of the ester group at about 1720 cm^{-1} and aliphatic C-H stretchings at about 2900 cm^{-1}. In

the region 1400-1590 cm^{-1}, vibrations ascribable to the symmetric and asymmetric stretchings of the carboxylate groups coordinated to the oxocluster metal ions can be detected [35]. The presence of low intensity vibrational bands at 1640 cm^{-1} hints to the presence of a small quantity of unreacted C=C double bonds, belonging to the oxocluster as well as to the monomer. The presence of these residual double bonds can be ascribed to the high steric hindrance of the oxoclusters, bearing 12 or 24 polymerizable groups which, once the copolymerization has been started, remain embedded in a stiff structure, thus preventing their reaction with further monomers.

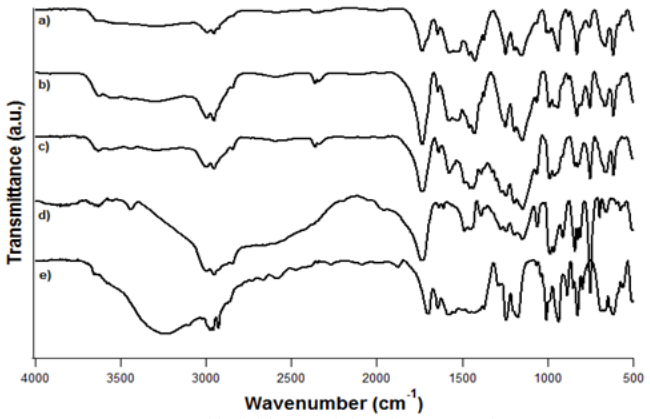

Fig. 1. FT-IR spectra of hybrids containing the Zr_6 oxocluster: [Zr_6MMA50T (a), Zr_6MMA100T (b) and Zr_6MMA200T (c)], compared to PMMA (d) and pure Zr_6 oxocluster (e). To allow an easier recognition of Zr_6-based oxocluster signals, the spectrum of the PMMA matrix was subtracted from their spectra (see Fig. S1).

The thermal behavior of the materials was then investigated by thermogravimetry. The recorded data confirm previous findings [26] about the improved thermal stability of the polymers cross-linked by the oxoclusters with respect to pristine PMMA, being the stability directly related to the oxocluster content (Fig. S2-S4). In the case of Zr-based oxoclusters (Fig.S2), thermogravimetric curves pointed out that a first weight loss (ca. 13%) occurs in the range 200-300°C, assigned to the removal of residual monomer and other adsorbed species, whereas at higher temperatures (300-450°C) a more relevant weight loss is observed, which has to be ascribed to the degradation of the hybrid matrix. At temperatures higher than 400°C, a last weight loss is detected, due to the decomposition of the organic part of the oxocluster to give ZrO_2, which is the detected inorganic residue observed (about 10-12% of the initial weight, in agreement to the amount of embedded oxocluster, each mole of which by decomposing produces 4 moles of zirconia).

The higher thermal stability of the hybrid materials is highlighted by the different degradation profiles (Fig. S2), being anticipated by about 80°C for the oxocluster-free PMMA. This effect is due to the enhanced cross-linking degree, induced by the oxocluster, as well as to the refractory layer produced, during combustion, by the inorganic domains as filler [36]. Accordingly, the highest thermal stability is displayed by Zr_4MMA50T, which is the sample characterized by the highest amount of incorporated oxocluster.

Upon storage in ethylacetate for 72 hours, the cross-linked materials swell (Table 1), the degree of swelling being related to the amount of incorporated oxocluster (i.e. the higher the amount of oxocluster, the higher the cross-linking, the lower the swelling degree). On the other hand, pristine PMMA and the hybrid materials embedding Zr_{12} completely dissolved. This latter observation can be related, as evidenced by the SS-NMR data (*vide infra*), to the fact that these bigger twelve-metals oxoclusters cross-link much less efficiently the polymer matrix, and they are loosely linked to it.

With the aim of obtaining further and more detailed structural information on the prepared hybrids, ^{13}C CP-MAS NMR spectra were recorded on Zr_4MMA50T, Zr_6MMA50T, Zr_{12}MMA50T, on the respective starting oxoclusters (Zr_4, Zr_6, Zr_{12}) and on PMMA. In Fig. 2 the spectra of all these samples are shown. The comparison with the spectra of pristine Zr_4 and PMMA provides information on the modifications occurring upon the hybrid formation. PMMA signals in the spectra of the hybrid and of pristine polymer appear substantially identical, indicating the similarity of the main structural features of PMMA in the presence or absence of the oxoclusters. In the spectrum of the pristine oxocluster Zr_4, every signal corresponding to a certain carbon nucleus appears structured in a variable number of peaks. Indeed, as shown by the crystal structure of Zr_4, [26,37] methacrylate groups occupy several spatially non-equivalent positions.

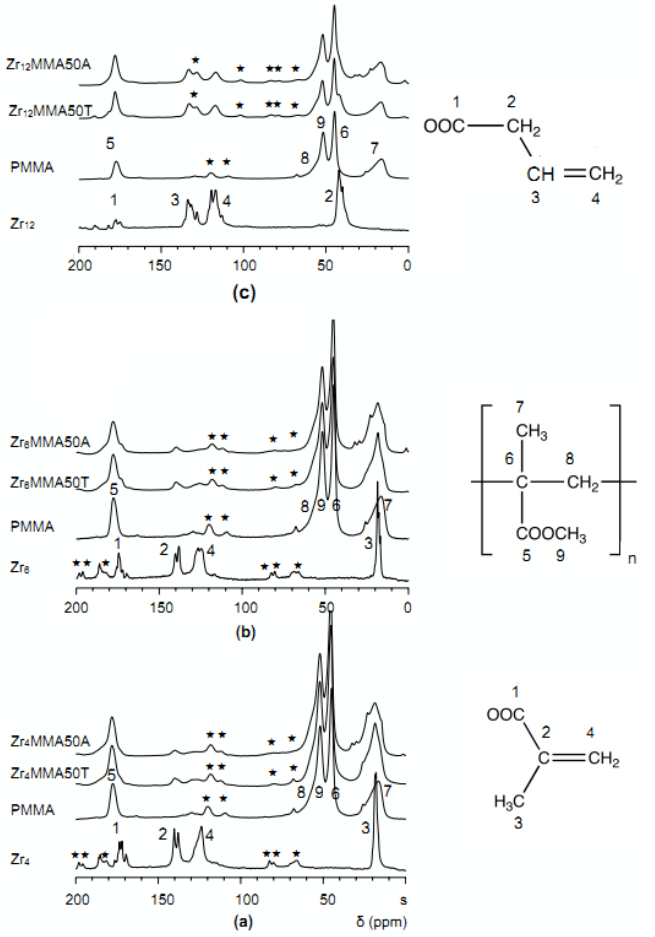

Fig. 2. ^{13}C CP-MAS spectra of (a) Zr_4, PMMA, hybrid Zr_4MMA50T before and after (Zr_4MMA50A) the reaction; (b) Zr_6, PMMA, hybrid Zr_6MMA50T before and after (Zr_6MMA50A) the reaction; (c) Zr_{12}, PMMA, hybrid Zr_{12}MMA50T before and after (Zr_{12}MMA50A) the reaction. The structures of the methacrylate group and methylmethacrylate, as monomers and as polymers are also reported, with the carbons numbering used for the signals assignment. Stars indicate spinning sidebands.

On the other hand, the broader signals observed for the embedded oxocluster suggest a higher degree of disorder for methacrylate groups dispersed in the polymer matrix. In detail, the broad signal at about 18 ppm arises from the superposition of the intrinsically broad methyl signal of PMMA and of the narrow one belonging to methyl groups on Zr_4. The main chain ^{13}C

signals of PMMA appear between 40 and 60 ppm, together with that of the methoxy carbon atoms [38–40].
Between 120 and 140 ppm, thanks to a spectral fitting procedure (the results of which are reported in Fig. S5), three signals can be recognized. Two of them, at 125 and 140 ppm, are ascribable to the olefinic carbons of Zr_4, and the last one, at about 130 ppm is due to olefinic carbon atoms of MMA (unreacted double bonds), and it is also observed in the spectrum of PMMA.
The COO ester group signal of PMMA is observed at 178 ppm, while two weak and broad shoulders, for the hybrids, are ascribable to the carboxylic carbon atoms of Zr_4. To estimate the amount of unreacted olefinic carbon atoms, and assess the polymerization degree, a quantitative ^{13}C DE-MAS spectrum of the hybrid was recorded (Fig.S5), from which it results that about 10-20% of MMA double bonds and about 50% of Zr_4 double bonds does not react, in agreement with FT-IR findings. This can also account for the TGA observation that 10-20% of the initial monomer is not incorporated, nevertheless hinting at a good degree of copolymerization.
The spectrum of Zr_6MMA50T is similar to that of Zr_4MMA50T, and all the comments done so far substantially hold true. A quantitative DE-MAS spectrum, due to the extremely long time required, was not recorded but, by applying approximate scaling factors (obtained from the spectra of Zr_4MMA50T) to the signals area of the CP-MAS spectrum, it was possible to estimate that also in this case about 50% of the oxocluster double bonds did not take part to the hybrid formation.
The case of Zr_{12}MMA50T is different since the oxocluster is functionalized with vinylacetate rather than methacrylate groups, and the potentially polymerizable groups are 24 instead of 12. Indeed, in the spectrum of the oxocluster, a signal at about 40 ppm, due to $OOCCH_2$- carbon is present and the peaks of the other carbon nuclei, which are characterized by a noticeable multiplicity, appear at slightly different chemical shifts with respect to Zr_4 and Zr_6. Concerning olefinic carbons of unreacted double bonds of both MMA and Zr_{12} it appears, from an approximate quantitative estimate (performed as previously discussed for Zr_6MMA50T), that more than 90% of the oxocluster double bonds does not react in the hybrid formation, output that also in this case can be traced back to steric hindrance, and which correlates well with the qualitative swelling experiments, showing that the hybrid materials embedding this oxocluster completely dissolve, hinting at a scarcely cross-linked structure.

3.2. Catalytic tests

Once thoroughly characterized from the chemico-physical and structural point of view, the obtained materials were tested in a model catalytic reaction, by exploiting the presence of Zr^{IV} and Hf^{IV} centers to activate hydrogen peroxide. A previous study on zirconium-based oxoclusters with interesting activity towards the oxygenation of sulfides and sulfoxides [12] has encouraged us to explore the double phase oxydesulfurization (ODS) of a model fuel in the presence of the polymeric materials embedding the oxoclusters. The oxidative removal of sulfur compounds may represent a sustainable alternative to the traditional hydrodesulfurization (HDS) process, since it can operate under less severe operating conditions, without involving high hydrogen pressures [42,43]. In this procedure, aromatic sulfides recalcitrant to traditional hydrodesulfurization treatments, such as dibenzothiophene (DBT), are oxidized, in a two-steps reaction, to the corresponding sulfoxide and then to the sulfone. Several studies described the use of catalytic systems involving the use of d^0 transition metals (Mo/W heteropolyanions or peroxometals associated to suitable surfactants, to obtain water-in-oil emulsions or ionic liquid phases [44-46], titania supported on silica[47], methyltrioxorhenium supported onto resins [48]) and H_2O_2, leading to deep desulfurization under mild conditions (ranging from room temperature to 80°C) in reaction times ranging from 30 min to few hours.
As a model fuel, we have used *n*-octane, while the oxoclusters are dissolved or dispersed in an extracting CH_3CN phase. In such conditions, DBT dissolves in equimolar amounts into *n*-octane and CH_3CN, and its oxidation products, being less soluble, are almost completely extracted into the most polar phase [20,49,50] (see reaction schemes in Fig. S6). Reactions were performed at T=65°C, in the presence of excess H_2O_2 (3.5 equivs). In Table 2 are reported the reaction yields, calculated with respect to the organic substrate (after 3 and 24 h), initial reaction rates (calculated at <30% substrate conversion), and the selectivities observed at 24 h.
Concerning polymer-free reactions, (entries 2-5 in Table 2), data show that the oxoclusters with lower nuclearity display a higher initial reactivity, with yields higher than 40% after 3h and a marked selectivity for sulfoxide oxidation. Hf_4 appears to be the most efficient one, with >70% yield after 24 h and 91% selectivity for the most oxidized product ($DBTO_2$). Due to the different structure and ligand set, leading to lower hydrolytic stability, Zr_{12} results the least reactive and shows a decreased tendency for sulfoxide oxidation (with <50% $DBTO_2$)[12].

Table 2. Oxidation of DBT by H_2O_2 activated by Zr/Hf oxoclusters.[a]

#	Catalyst	Yield % 3 h	Yield % 24 h	R_0 (μmol L^{-1} s^{-1})	Selectivity SO:SO_2[b]
1[c]	-	1	3	-	100:0
2	Zr_4	49	60	0.65	17:83
3	Zr_6	47	52	0.51	28:72
4	Zr_{12}	20	34	0.13	53:47
5	Hf_4	40	73	0.42	9:91
6	Zr_4MMA50T	44	84	0.64	5:95
7	Zr_6MMA50T	53	66	0.84	4:96
8	Zr_{12}MMA50T	25	31	0.36	21:79
9	Hf_4MMA50T	41	89	0.33	6:94
10	Zr_4MMA100T	43	81	0.41	11:89
11	Zr_6MMA100T	43	72	0.72	6:94
12	Zr_{12}MMA100T	29	43	0.21	15:85

[a] Reaction conditions: 1 mL *n*-octane containing 0.01 M DBT, 1 mL CH_3CN containing 0.035 M H_2O_2 (added as 30% aqueous solution) and 15% mol catalyst, T=65°C. [b] DBT is equally distributed in both phases, while DBTO and $DBTO_2$ are completely extracted in CH_3CN; [c] blank reaction without oxoclusters. The addition of methacrylic acid gave analogue results.

Fig. 3a reports the kinetic behavior observed for Zr_4. As for the other homogeneous catalysts (Fig. S7-S17), the kinetic profile is characterized by a steady state regime for the intermediate product, followed by a plateau region. Indeed, due the concurrent

oxidant decomposition, the reactions level-off after an initial burst of reactivity.

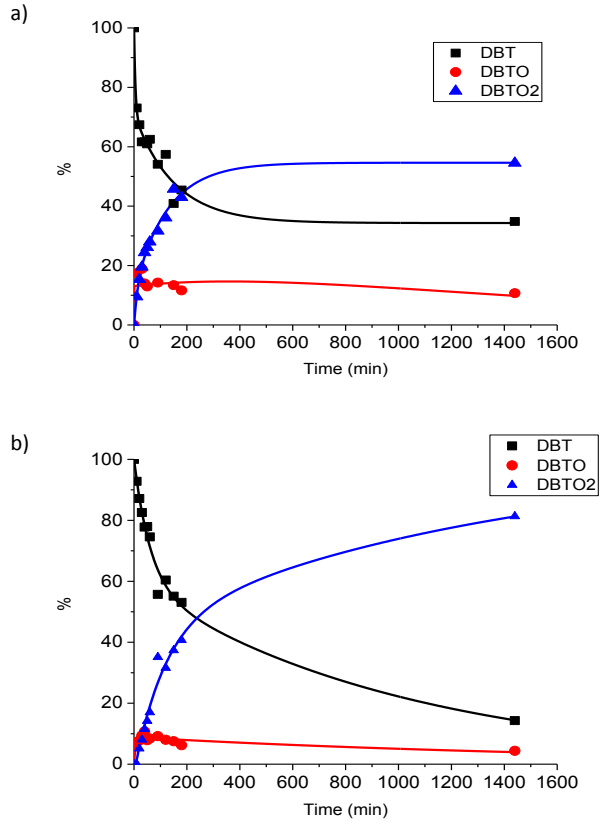

Fig. 3. Kinetic profiles for the oxidation of DBT by H_2O_2 in the presence of (a) Zr_4 and (b) Zr_4MMA50T. DBT concentration has been calculated as the total amount, dissolved both in *n*-octane and in acetonitrile. DBTO and $DBTO_2$ concentrations refer to the acetonitrile phase.

The heterogeneous catalytic tests (entries 6-12 in Table 2) were performed by using grinded polymers. The data highlight a better performance for all polymeric formulations, which retain the initial reactivity observed in homogeneous solution, without showing deactivation at longer reaction time. For example, Zr_4MMA50T reaches 84% yield (vs 60% in homogenous conditions), while Hf_4MMA50T yield rises to 89% (vs 73% in homogenous conditions). The higher reactivity for the embedded oxoclusters is likely due to the enhanced hydrolytic stability of the oxoclusters, coupled with an advantageous enrichment of the substrates (DBT, DBTO) within the polymeric matrix, which favours the conversion to $DBTO_2$ [20]. In addition, only a minor H_2O_2 decomposition is observed in such conditions.

Figure 3b reports the kinetic profile obtained in the presence of Zr_4MMA50T, which displays the best performances, in terms of initial reaction rate and selectivity, among the hybrid materials. The smaller improvements observed for Zr_{12}-based copolymers are likely attributed to the lower incorporation efficiency of this sterically hindered oxocluster in the polymer backbone, as evidenced by swelling experiments and ^{13}C NMR quantitative data.

Despite the much higher swelling degree (Table 1), the hybrids with a oxocluster:MMA molar ratio of 1:100 (100T) display only a minor difference in reactivity with respect to 50T ones. In addition, selectivity towards $DBTO_2$ is decreased, and a parallel unproductive H_2O_2 consumption is observed. This can be due to a lower accessibility to the oxoclusters, as well as to H_2O_2 scavenging by the higher amount of unreacted MMA double bonds.

Porous polymers have been finally prepared, upon addition of a mixture of porogenic solvents (1,4-butandiol and 2-propanol) to the polymerization reaction. In this case, despite the higher accessibility of the oxoclusters, resulting from higher surface area, the reaction efficiency is lower (<42% conversion in 24h). On the other hand, as confirmed by the identical reaction rate observed at different experimental stirring speed (500 or 1000 rpm), the reaction rate seems to be not limited by the diffusion of the reactants within the polymer matrix.

This outcomes highlight the key role of an optimal oxocluster distribution/cross-linking to avoid undesired reactions involving the oxoclusters and the oxidant.

3.3. Recovery, reuse and structural assessment of the hybrid materials

To confirm the positive effects of the polymeric matrix against possible changes in both structure and/or composition of the catalytic materials, we have performed further analyses on the hybrid materials after catalysis. It should be underlined that these changes could be induced by degradation phenomena ascribed either to the polymer matrix or rather to the oxocluster: (i) leaching of the oxocluster from the polymer matrix; (ii) hydrolysis/condensation or oxidation reactions of the oxoclusters; (iii) oxidation of the polymer matrix. Whereas the first possible degradation phenomenon is less probable, being the oxocluster covalently linked to the matrix, the others have deserved a closer insight. The studies were focused on Zr_4MMA50T, which exhibits the best catalytic performances. The stability of the oxocluster was investigated by XAS, which has been already assessed as a powerful tool to study the stability of inorganic building blocks in hybrid materials [51], and to provide details on the local chemical environment of the metal species (in this case Zr). In particular, this technique was useful to provide preliminary insights on the formation of peroxospecies when the pure oxocluster is incubated with a strong H_2O_2 excess [12]. Fig. 4 reports the k^3-weighted EXAFS functions (a) and the corresponding Fourier transforms (b, phase-shifted) for Zr_4 and the 1:50 hybrid before (Zr_4MMA50T) and after catalysis (Zr_4MMA50A). As it can be noted, the EXAFS functions do not present significant variations among the different samples, with only a minor difference at about 7 $Å^{-1}$ between the pure oxocluster and the two hybrids. Such minor changes are more evident in the Fourier transforms, in particular in the first shell range (1.3-2.7 Å). This first shell signal is divided in two peaks, representing the two Zr-O distances expected (see Table 3), and shows only a slight decrease in the second band intensity (at 2.25 Å) for the hybrid Zr_4MMA50T materials, with respect to the pure Zr_4. The retention of all spectral features evidences that when the oxocluster is embedded in the polymeric matrix only minor structural changes occur in its core (SS-NMR highlighted a certain disorder affecting the methacrylate groups). The signal at 3.5 Å, corresponding to a Zr-Zr distance, does not show any variation and suggests that the oxocluster retains its structure during catalysis and it is not decomposed. These findings are further confirmed by the fitting of the experimental spectra with theoretical models based on the crystal structure, as reported in Table 3. The modeling does not evidence any significant change between the different samples, thus confirming the stability of the cluster during the catalytic process.

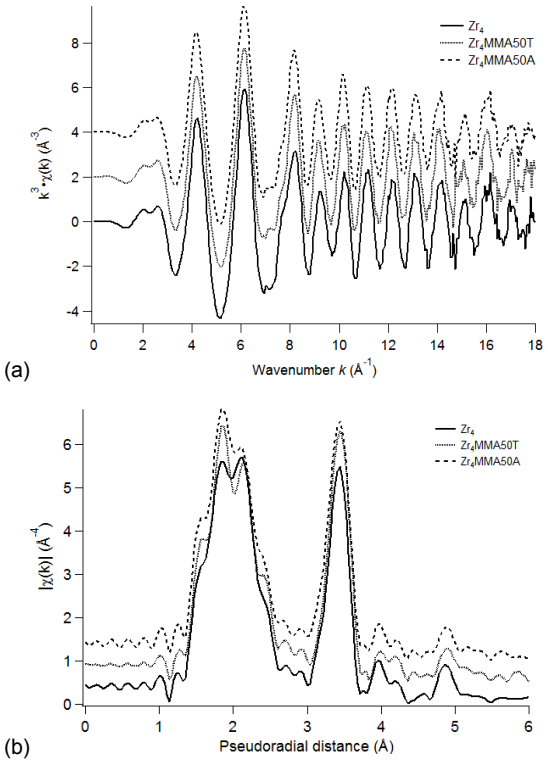

Fig. 4. a) k^3-weighted EXAFS functions (at Zr K-edge) and b) corresponding Fourier transforms for Zr_4 (solid line), Zr_4MMA50T (dotted) and Zr_4MMA50A (dashed).

Table 3. Numeric results from fitting the experimental EXAFS spectra with theoretical model Zr_4.

Sample	Abs-Bs[a]	Coordination number	R (Å) [b]	σ^2 (Å^2) [c]
Zr_4 (XRD)[24]	Zr-O	4.5	2.14	-
	Zr-O	3.0	2.23	-
	Zr-Zr	2.5	3.59	-
Zr_4	Zr-O	4.5±0.7	2.12±0.02	0.004±0.001
	Zr-O	6.2±0.9	2.25±0.02	0.004±0.001
	Zr-Zr	2.8±0.8	3.52±0.01	0.005±0.001
Zr_4MM50T	Zr-O	4.8±0.6	2.11±0.02	0.004±0.001
	Zr-O	6.0±0.7	2.25±0.01	0.004±0.001
	Zr-Zr	3.8±0.9	3.52±0.01	0.006±0.001
Zr_4MM50A	Zr-O	5.3±0.7	2.12±0.02	0.005±0.001
	Zr-O	6.1±0.7	2.26±0.01	0.005±0.001
	Zr-Zr	3.4±0.8	3.53±0.01	0.005±0.001

[a] Abs=absorber atom, Bs=backscattering atom [b] Distance Abs-Bs [c] Debye-Waller factor

A further insight into the microstructure of the hybrid materials the oxocluster distribution in the polymer matrix, as well as the effect of the catalytic process on the microstructure was pursued by Small Angle X-ray Scattering (SAXS). Fig. 5 shows SAXS data of four samples: Zr_4MMA50T before and after catalysis (Zr_4MMA50A), Zr_6MMA50T and Zr_4MMA50P (with porogenic solvents). In a log-log-plot the SAXS data exhibit an almost perfect Porod law, i.e. they obey $I(s) \propto 1/s^4$ at larger values of the modulus of the scattering vector s, indicating the presence of objects (oxoclusters) possessing a significantly different electron density than the surrounding matrix.

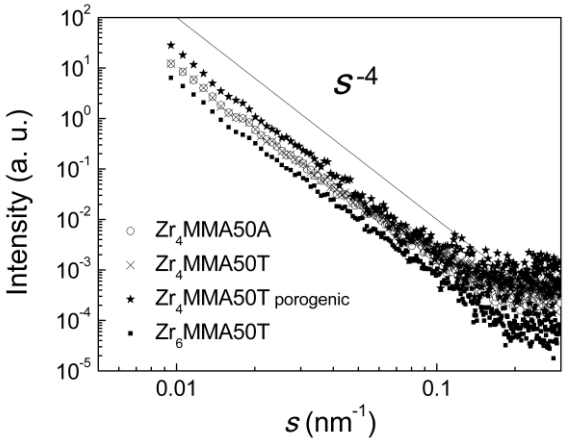

Fig. 5. SAXS data collected for various 1:50 hybrids.

The fact that no maxima in I(s) are observable indicates the lack of long-range and short-range order and thus are in conformity with a homogeneous statistic distribution of the oxoclusters or small aggregates of oxoclusters within the polymeric matrix. However, the absence of maxima and the SAXS data measured at quite small values of s allow for the analysis by the Guinier law $I(s) \propto \exp(-(4\pi^2 s^2 R_g^2)/3)$ (where R_g is the radius of gyration), being applicable as asymptotic behavior in the region of small s values. Indeed, the SAXS data of the four samples shown in Fig. 5 fulfill the Guinier law at small s, and for all samples an average value of R_g ca. 10 nm can be extracted from fitting the SAXS data at small s. This value seems to be quite large at a first glance, but is in conformity with a diameter of ca. 2 nm, i.e. in the range expected for the oxoclusters. Thus, a value of R_g = 10 nm indicates the formation of small aggregates of several oxoclusters. Interestingly, the SAXS data are almost identical for all of these samples. Thus, the cluster size does not change during the catalytic reaction, i.e. these results further confirm that the oxoclusters remain chemically intact, which is also in agreement with XAS data.

Concerning FT-IR data of Zr_6MMA50T, the more striking difference pointed out between the materials before and after the catalysis is the decrease of the intensity of the band due to double bonds, which is ascribed to their oxidation in the presence of H_2O_2 (Fig. S18). On the other hand, the rRaman spectra of Zr_6MMA50T, collected before and after the reaction, do not display any change, thus confirming its stability under oxidative conditions. Nevertheless, the rRaman spectra collected after addition of H_2O_2, in acetonitrile, display minor changes between 800 and 900 cm^{-1}, i.e. the region where peroxometal bonds give a resonance signal (Fig. S19).

The ^{13}C SS-NMR spectra of Zr_4MMA50T, Zr_6MMA50T and Zr_{12}MMA50T recovered after the catalysis are shown in Fig. 2 They can be collectively commented since the same effects are observed. Firstly, it can be noticed that the signals of PMMA are substantially unchanged indicating that the catalytic process does not strongly alter the polymeric backbone. The most evident effect is the appearance of four relatively narrow peaks at 15.0, 23.0, 29.8, 36.2 ppm (the first two superimposed to the broad methyl signal) and one at about 1.2 ppm, which must be ascribed to residual octane and acetonitrile, respectively. No signals due to

DBT or to its oxidation products were observed. Comparing the spectra before and after the catalysis it is also possible to observe a slight intensity increase of the PMMA signals between 40 and 60 ppm with respect to the other signals, which could be tentatively ascribed to a slight stiffening of the polymer main chain, and a slight decrease of the signals due to the olefinic carbon atoms, in agreement with FT-IR outcomes.

As far as the morphology of the hybrids is concerned, the specific surface area of the materials (Zr_4MMA50T), measured by BET analysis, remains practically unchanged, from 2.1 m^2g^{-1} before the catalysis to 1.9 m^2g^{-1} after the catalysis. The morphology of the hybrid materials was also investigated by SEM. While the samples show a smooth surface (interrupted only by cracks due to drying process), the presence of the porogenic solvents (Fig.S20) induces an increased roughness of the hybrid interface, and pores in the order of hundreds of nm diameter can be observed.

To evaluate the retention of the catalytic activity, the reaction mixture containing Zr_4MMA50T was recharged (three times, at t=24 h intervals) with further DBT and with H_2O_2. The second run showed a 50% decrease of the catalytic efficiency, in terms of total sulfur removal, these performances were found to stabilize during next runs (Fig. S21). On the other hand, much better performances were obtained after removal and washing of the catalyst from the reaction mixture, in order to remove the adsorbed products. In this case, very similar performances were observed, with the same initial rate (R_0=3.1x10^{-7} mol L^{-1} s^{-1}), 80% yield in 24 h and 1:99 SO:SO_2 selectivity (Fig. S22). The absence of catalyst leaching from the bulk polymer was then assessed by removing the hybrid material from the reaction mixture after two hours of reaction. Although some DBTO can still form from the uncatalyzed oxidation (see Table 2), the observation of a constant concentration of $DBTO_2$ is in agreement with the absence of active metal species in solution. Accordingly, a negligible amount of Zr (<250 ppb) was observed by ICP-MS in both filtrated phases.

Such performances confirm the positive effects of the polymeric matrix, which, beside allowing an easy recycling, improves the stability and the catalytic efficiency.

4. Conclusions

A set of novel polymethyl methacrylate polymers, covalently reinforced by polymerizable Zr/Hf oxoclusters has been prepared and used for the first time as stable heterogeneous catalysts.

By a combined investigation, based on FT-IR and ^{13}C SS-NMR spectroscopies, it was possible to verify the structure of the oxoclusters and of the hybrids, thus revealing and quantifying a fraction of unreacted double bonds. SS-NMR data also evidenced how this fraction is higher for Zr_{12}-based hybrids, due to the elevated steric hindrance characterizing this cluster. Accordingly, the lower cross-linking efficiency for Zr_{12}-based hybrids was also confirmed by swelling experiments. Thermogravimetry highlighted an increased thermal stability for hybrid materials, compared to pristine PMMA.

The catalytic efficiency of the oxoclusters was demonstrated in the sulfoxidation of dibenzothiophene (DBT) by H_2O_2, in a biphasic (*n*-octane/CH_3CN) system, as an example of sustainable oxydesulfurization (ODS), where sulfur content can be reduced from 300 to 25-65 ppm in 24 h at 65°C. The heterogeneous catalysts show an enhanced activity, in terms of reaction yield and selectivity, with respect to the soluble oxoclusters, pointing to a major role of the polymeric matrix in shaping a suitable environment for implementing catalyst stability and reaction selectivity. The comparison between FT-IR, rRaman and SS-NMR spectra recorded before and after the catalysis shows indeed a substantial stability of the hybrids. The stability of the clusters throughout the catalytic reaction was also evidenced by XAS experiments. Neither the XANES nor EXAFS regions showed any significant difference after catalysis, being the spectral features of the best performing material very similar to those of pure Zr_4 cluster. Thanks to this stability, Zr_4MMA50T could be recovered and recycled with no loss of activity.

Despite the lower reactivity, with respect to recent literature reports on ODS process [44-50], our results represent a fundamental step further toward the development of a novel class of metal oxoclusters-based heterogeneous catalysts. On the other hand, the possibility to modify the properties of the hybrids, depending on the oxocluster nature and on the addition of suitable additives was demonstrated. Further investigations are required to optimize the morphology and the affinity towards the substrates, while addressing incomplete cross-linking and solubility issues.

Acknowledgments

Dr. Ingrid Zenke (Max-Planck Institute of Colloids and Interfaces) is thanked for performing the SAXS measurements, Dr. Roberta Saini (University of Padova) is acknowledged for TGA-DSC measurements and Dr. Denis Badocco (University of Padova) is acknowledged for ICP-MS measurements. The Italian Foreign Affairs Ministry (Ministero degli Affari Esteri, MAE, Italy) and the National Research Council (CNR, Italy) are gratefully acknowledged for the financial support of this work in the framework of the "Progetto Grande Rilevanza Italia-Slovenia 2013". The University of Padova, the Italian Consortium INSTM are acknowledged for providing money and equipment. We would like to thank Dr. G. Aquilanti and Dr. L. Olivi for their support during EXAFS measurements and the European Community for financial support in activities under the EU Calipso Programme. The research leading to these results has received funding from the European Community's Seventh Framework Program (FP7/2007-2013) under grant agreement n° 226716. A.S and M.C. acknowledge the financial support from Fondazione Cariparo (Progetto Dottorati di Ricerca PARO118894/11).

References and notes

[1] Schubert U., *Macromol. Symp.* **2008**, *267*, 1–8.
[2] Schubert U., *Chem. Soc. Rev.* **2011**, *40*, 575–582.
[3] Albinati A., Faccini F., Gross S., Kickelbick G., Rizzato S., Venzo A., *Inorg. Chem.* **2007**, *46*, 3459–3466.
[4] Lane B.S., Burgess K., *Chem. Rev.* **2003**, *103*, 2457–2473.
[5] Arends I.W.C.E., Conte V., Licini G., in *Innov. Catal. Org. Synth. Oxidation, Hydrog. C-X Bond Form. React.*, **2012**, pp. 77–102.
[6] Mal S.S., Nsouli N.H., Carraro M., Sartorel A., Scorrano G., Oelrich H., Walder L., Bonchio M., Kortz U., *Inorg. Chem.* **2010**, *49*, 7–9.
[7] Jahier C., Mal S.S., Kortz U., Nlate S., *Eur. J. Inorg. Chem.* **2010**, 1559–1566.
[8] Carraro M., Nsouli N.H., Oelrich H., Sartorel A., Sorarù A., Mal S.S., Scorrano G., Walder L., Kortz U., M. Bonchio, *Chem. - A Eur. J.* **2011**, *17*, 8371–8378.
[9] Li D., Han H., Wang Y., Wang X., Li Y., Wang E., *Eur. J. Inorg. Chem.* **2013**, 1926–1934.
[10] Kholdeeva O.A., Maksimovskaya R.I., *J. Mol. Catal. A Chem.* **2007**, *262*, 7–24.
[11] Al-Kadamany G., Mal S.S., Milev B., Donoeva B.G., Maksimovskaya R. I., Kholdeeva O.A., Kortz U., *Chem. - A Eur. J.* **2010**, *16*, 11797–11800.
[12] Faccioli F., Bauer M., Pedron D., Sorarù A., Carraro M., Gross S., *Eur. J. Inorg. Chem.* **2015**, *2015*, 210–225.

[13] Bahrami K., *Tetrahedron Lett.* **2006**, *47*, 2009–2012.
[14] Gross S., *J. Mater. Chem.* **2011**, *21*, 15853-15861.
[15] Carraro M., Gross S., *Materials.* **2014**, *7*, 3956–3989.
[16] Kholdeeva O.A., Maksimchuk N.V., Maksimov G.M., *Catal. Today*, **2010**, 107–113.
[17] Biffis A., Zecca M., Basato M., *J. Mol. Catal. A Chem.* **2001**, *173*, 249–274.
[18] Bonchio M., Carraro M., Scorrano G., Fontananova E., Drioli E., *Adv. Synth. Catal.* **2003**, *345*, 1119–1126.
[19] Carraro M., Gardan M., Scorrano G., Drioli E., Fontananova E., Bonchio M., *Chem. Commun.*. **2006**, 4533–4535.
[20] Carraro M., Fiorani G., Mognon L., Caneva F., Gardan M., Maccato C., Bonchio M., *Chem. Eur. J.* **2012**, *18*, 13195–13202.
[21] Bonchio M., Carraro M., Gardan M., Scorrano G., Drioli E., Fontananova E., in *Top. Catal.*, **2006**, pp. 133–140.
[22] Campos-Martin J.M., Capel-Sanchez M.C., Fierro J.L. G., *Green Chem.* **2004**, *6*, 557–562.
[23] Al-Shahrani F., Xiao T., Llewellyn S.A., Barri S., Jiang Z., Shi H., Martinie G., Green M.L.H., *Appl. Catal. B Environ.* **2007**, *73*, 311–316.
[24] Ballistreri F.P., Tomaselli G.A., Rosa V., Toscano M., Conte V., Di Furid F., **1991**, 6209–6212.
[25] Gross S., Kickelbick G., Puchberger M., Schubert U., *Monatshefte fur Chemie* **2003**, *134*, 1053–1063.
[26] Trimmel G., Gross S.,. Kickelbick G, Schubert U., in *Appl. Organomet. Chem.*, **2001**, pp. 401–406.
[27] Kickelbick G., Wiede P., Schubert U., *Inorganica Chim. Acta* **1999**, *284*, 1–7.
[28] Puchberger M., Kogler F.R., Jupa M., Gross S., Fric H., Kickelbick G., Schubert U., *Eur. J. Inorg. Chem.* **2006**, *2006*, 3283–3293.
[29] Trimmel G., Fratzl P., Schubert U., *Chem. Mater.* **2000**, *12*, 602–604.
[30] Ravel B., Newville M., *J. Synchrotron Radiat.* **2005**, *12*, 537–541.
[31] Allen G., Bevington J.C., in *Compr. Polym. Sci. Suppl.*, Pergamon Press, **1989**.
[32] Elias H.G., Makromoleküle: Struktur, Eigenschaften, Synthesen, Stoffe, Hüthig & Wepf, Basel, **1990**.
[33] Mayer C.R., Thouvenot R., Lalot T., *Chem. Mater.* **2000**, *12*, 257–260.
[34] Graziola F., Girardi F., Bauer M., Di Maggio R., Rovezzi M., Bertagnolli H., Sada C., Rossetto G., Gross S., *Polymer.* **2008**, *49*, 4332–4343.
[35] Nakamoto K., Infrared and Raman Spectra of Inorganic and Coordination Compounds: Part B: Applications in Coordination, Organometallic, and Bioinorganic Chemistry, **2008**.
[36] Kogler F.R., Schubert U., *Polymer.* **2007**, *48*, 4990–4995.
[37] Walther P., Puchberger M., Kogler F.R., Schwarz K., Schubert U., *Phys. Chem. Chem. Phys.* **2009**, *11*, 3640–3647.
[38] Schaefer J., Stejskal E.O., Buchdahl R., *J. Macromol. Sci. - Phys.* **1977**, *B13*, 384–405.
[39] Eijkelenboom A.P.A.M., Maas W.E.J.R., Veeman W.S., Buning G.H.W., Vankan J.M.J., *Macromolecules* **1992**, *25*, 4511–4518.
[40] Noyori R., Aoki M., Sato K., *Chem. Commun.* **2003**, 1977–1986.
[41] Haw K.G., Bakar W.A.W.A., Ali R., Chong J.F., Kadir A.A.A., *Fuel Process. Technol.* **2010**, *91*, 1105–1112.
[42] Zhu W., Li H., Jiang X., Yan Y., Lu J., He L., Xia J., *Green Chem.* **2008**, *10*, 641-646.
[43] Jiang Y., Zhu W., Li H., Yin S., Liu H., Xie Q., *ChemSusChem* **2011**, *4*, 399–403.
[44] Sachdeva T.O., Pant K.K., *Fuel Process. Technol.* **2010**, *91*, 1133–1138.
[45] Li C., Jiang Z., Gao J., Yang Y., Tian F., Sun F., Sun X., Ying P., *Chem. Eur. J.* **2004**, *10*, 2277–2280.
[46] Zhu W., Zhu G., Li H., Chao Y., Du D., Wang Q., Zhao Z., *Fuel Process. Technol.* **2013**, *106*, 70–76.
[47] Frailea J. M., Gil C., Mayoral J. A., Muel B., Roldán L., Vispe E., Calderón S., Puente F., *Appl. Catal. B: Environ.* **2016**, *180*, 680–686.
[48] Di Giuseppe A., Crucianelli M., De Angelis F., Crestini C., Saladino R., *Appl. Catal. B: Environ.* **2009**, *89*, 239–245.
[49] Yazu K., Yamamoto Y., Furuya T., Miki K., Ukegawa K., *Energy Fuels* **2001**, *15*, 1535–1536.
[50] Capel-Sanchez M.C., Perez-Presas P., Campos-Martin J.M., Fierro J.L.G., *Catal. Today* **2010**, *157*, 390–396.
[51] Gross S., Bauer M., *Adv. Funct. Mater.* **2010**, *20*, 4026–4047.